Research article

vCPP2319 interacts with metastatic breast cancer extracellular vesicles (EVs) and transposes a human blood-brain barrier model

Filipa D. Oliveira [a], Marco Cavaco [a], Tiago N. Figueira [a], Patrícia Napoleão [a], Javier Valle [b], Vera Neves [a], David Andreu [b], Miguel A.R.B. Castanho [a],*

[a] *Gulbenkian Institute for Molecular Medicine, Faculdade de Medicina da Universidade de Lisboa, Av. Prof. Egas Moniz, Lisbon, 1649-028, Portugal*
[b] *Department of Medicine and Life Sciences, Pompeu Fabra University, Barcelona Biomedical Research Park, 08003, Barcelona, Spain*

ARTICLE INFO

ABSTRACT

Brain metastases (BM) are frequently found in cancer patients and, though their precise incidence is difficult to estimate, there is evidence for a correlation between BM and specific primary cancers, such as lung, breast, and skin (melanoma). Among all these, breast cancer is the most frequently diagnosed among women and, in this case, BM cause a critical reduction of the overall survival (OS), especially in triple negative breast cancer (TNBC) patients. The main challenge of BM treatment is the impermeable nature of the blood-brain barrier (BBB), which shields the central nervous systems (CNS) from chemotherapeutic drugs. Extracellular vesicles (EVs) have been proposed as ideal natural drug carriers and these may exhibit some advantages over synthetic nanoparticles (NPs). In this work, we isolate breast cancer-derived EVs and study their ability to carry vCPP2319, a peptide with dual cell-penetration and anticancer activities. The selective cytotoxicity of anticancer peptide-loaded EVs towards breast cancer cells and their ability to translocate an *in vitro* BBB model are also addressed. Overall, it was possible to conclude that vCPP2319 naturally interacts with breast cancer-derived EVs, being retained at the surface of these vesicles. Moreover, the results revealed a cytotoxic activity for peptide-loaded EVs similar to that obtained with the peptide alone and the ability of peptide-loaded EVs to translocate an *in vitro* BBB model, which contrasts with the results obtained with the peptide alone. In conclusion, this work supports the use of EVs in the development of biological drug-delivery systems (DDS) capable of translocating the BBB.

1. Introduction

Brain metastases (BM) are a major clinical complication frequently found in patients with advanced stages of cancer, leading to

cognitive impairment, and reduced quality of life and lifespan [1,2]. BM are more frequently diagnosed than primary brain tumors and their incidence is increasing mainly due to improvements in diagnosis – allowing for early detection of BM – and treatment - increasing patient lifespan though also expanding the time frame for BM development [2,3]. Despite the advances in diagnosis and treatment, the prognosis remains poor, with extremely low 2-year overall survival [1,4,5]. The precise incidence of BM is not accurately determined but evidence from autopsy studies revealed an association between BM and certain primary cancers, namely lung, breast and skin (melanoma) [2,5]. Breast cancer is the most frequently diagnosed cancer among women and the overall survival (OS) of patients with breast cancer BM was described to be less than 1 year, which decreases to less than 6 months for triple negative breast cancer (TNBC) patients [6,7].

One of the main challenges in treatment of BM resides in the blood-brain barrier (BBB) and its impermeable nature, which protects the central nervous system (CNS) but also turns it into a "sanctuary" where metastatic tumor cells settle and proliferate, shielded from chemotherapeutic drugs [3,8]. Several invasive and non-invasive approaches have been investigated to overcome this limitation and improve drug delivery to the brain [9]. Invasive strategies usually have high costs, which together with the need for follow-ups, hardware complications and brain damage risks significantly compromise patient compliance [9]. Non-invasive strategies with targeted drug delivery are therefore advantageous and preferable. A recent review on the pharmacoeconomical impact of the use of nanocarriers as drug delivery systems (DDS) for cancer treatment pointed out that nanoencapsulation may improve the bioavailability, solubility, selectivity and pharmacokinetic (PK) profile of drugs, as well as facilitate biological barrier translocation, storage and *in vivo* stability [10]. All these improvements result in more efficient formulations, and reduction of dosage and toxicity, therefore reducing side effects and costs, and ultimately leading to a favorable impact on patients' compliance [10]. Nanoparticles (NPs) have been promoted as novel strategies for drug delivery with improved efficacy and safety, such as the pegylated liposomal formulations of doxorubicin used to treat metastatic breast cancer (MBC) [11,12]. On the down side, unspecified cytotoxicity and rapid elimination by the phagocytic system are listed as frequent disadvantages of NPs [11].

Extracellular vesicles (EVs) have been portrayed as ideal natural DDS [13–15]. EVs are a broad population of vesicles naturally found in body fluids such as blood, and can be generally divided into two classes: exosomes and shedding microvesicles (MVs) [16,17]. This classification relies essentially on different biogenesis pathways and sizes [16,18,19]. Exosomes (30–120 nm) are initially formed as intraluminal vesicles (ILVs) within a multivesicular body (MVB), which then fuses with the plasmatic membrane, releasing its content into the extracellular space [15,16,18,20]. MVs are generally larger than exosomes (100–1000 nm) and assembled directly at the cell membrane level through the regulated outward budding of small membrane domains [16,18]. Exosomes, in particular, have received much attention in the last decades since they were found to be key participants in intercellular communication [21,22]. Moreover, intrinsic characteristics such as small size, native membrane components (protein and lipids), high biocompatibility and stability, and low immunogenicity and toxicity, confer exosomes evident advantages over synthetic DDS [21–23]. In particular, tumor-derived exosomes (TDEs) are easy to collect, being found at high concentration in malignant effusions, and are also described to interact more promptly with cancer cells due to their unique lipid composition [15,24]. Several works have explored the use of cancer-derived exosomes as DDS to effectively deliver anticancer drugs in what may be considered a "Trojan horse" approach [14,15, 24–27]. However, given their key role in metastatic cancer progression, the use of TDEs as DDS must be considered with caution. In this sense, many strategies have been used to engineer exosomes, aiming for the development of optimized DDS with effective anticancer activity, and showing promising results that constitute evidence of their potential in cancer treatment [22,24,28,29]. As a noteworthy example, a recent report on the encapsulation of pegylated liposomal doxorubicin in TDEs showed that not only did EVs fuse preferentially with cancer cells, but that they displayed enhanced therapeutic retention in tumor tissues [24].

In this work, we explored the use of EVs isolated from TNBC cells MDA-MB-231 to deliver vCPP2319, a peptide whose mode of action combines cell-penetrating (CPP) and anticancer (ACP) activities [30,31] resulting in tumor cell membrane-crossing properties, with subsequent impact on intracellular biomechanics [30]. As potential sources of novel drug leads, peptides are getting increased attention due to features such as small size –relative to proteins– and high specificity [32]. Nonetheless, their use in clinics still faces challenges such as instability, immunogenicity or limited ability to cross biological barriers such as the BBB [32,33]. A possible strategy to overcome these limitations is encapsulation of the peptide drug into carrier systems such as –in the present work–exosomes and other EVs that shield the peptide from early degradation until specific delivery to its target.

2. Experimental section/methods

2.1. Reagents

Fmoc-protected amino acids, Fmoc-Rink amide (MBHA) resin, 2-(1H-benzotriazol-1-yl)-1, 1, 3, 3–tetramethyluronium hexafluorophosphate (HBTU), and N-hydroxybenzotriazole (HOBt) were from Iris Biotech GmbH (Marktredwitz, Germany). HPLC-grade acetonitrile (ACN), peptide-synthesis grade N,N-dimethylformamide (DMF), dichloromethane, N,N-diisopropylethylamine (DIEA), N,N-diisopropylcarbodiimide, trifluoroacetic acid (TFA), and triisopropylsilane (TIS) were from Carlo Erba Reagents GmbH (Sabadell, Spain). Quasar® 670 was obtained from LGC Biosearch Technologies (Hoddesdon, UK). Dulbecco's Modified Eagle Medium (DMEM), DMEM:F12, heat-inactivated fetal bovine serum (FBS), penicillin and streptomycin solution, trypsin (TrypLE Express enzyme), trypsin-EDTA and exosome-depleted FBS (dFBS) were obtained from Thermo Fisher Scientific (Waltham, MA, USA). Mammary Epithelial Basal Medium (MEBM) and the SingleQuots hydrocortisone, bovine pituitary extract (BPE), epidermal growth factor human recombined (rhEGF), and recombinant human insulin were purchased as the clonetics MEGM™ BulletKit™ from Lonza Group AG (Basel, Switzerland). Cholera toxin from *Vibrio cholera*, trypsin inhibitor from *Glycine* max (soybean), glutaraldehyde solution (50 % in water), endothelial growth supplement (ECGS) and dimethyl sulfoxide (DMSO) suitable for cell culture were obtained from Sigma-Aldrich

(Madrid, Spain). DMSO spectrophotometric grade was purchased from Merck as Uvasol® DMSO for UV spectroscopy (≥99.8 %). MTT (3-(4,5-dimethylthiazol-2-yl)-2,5-diphenyltetrazolium bromide) salt was purchased from Invitrogen™ (Carlsbad, CA, USA). CellTiter-Blue® Reagent was obtained from Promega (Madrid, Spain). 4-(2-[6-(dioctylamino)-2-naphthalenyl]ethenyl)-1-(3-sulfopropyl) pyridinium inner salt (di-8-ANEPPS) probe was purchased from Sigma-Aldrich. vCPP2319 was purchased from Bachem AG (Bubendorf, Switzerland) with a purity of >95 %. The peptide was synthesized with a N-terminal free amine and an amidated C-terminal. Total exosome isolation (from cell culture media) reagent was purchased from Invitrogen™. Micro BCA protein assay kit was obtained from Thermo Fisher Scientific (Waltham, Massachusetts, EUA). Antibodies Alexa Fluor® 647 Mouse anti-Human CD63, PerCP-Cy™ 5.5 Mouse anti-Human CD105 and anti-EpCAM PE, the dye CFSE (carboxyfluorescein diacetate succinimidyl ester) and PE Mouse IgG1, κ Isotype Control were obtained from BD Biosciences (Franklin Lakes, Nova Jersey, EUA). The nanobeads calibration kit was purchased from Bangs Laboratories, Inc. Biacore sensor chip regeneration reagents 3-[(3-cholamidopropyl) dimethylammonio]-1-propanesulfonate (CHAPS), octyl β-D-glucopyranoside and methanol were from Sigma, and sodium hydroxide (NaOH) and sodium dodecyl sulfate (SDS) were from GE Healthcare (Little Chalfont, UK).

2.2. Peptide synthesis

vCPP2319 (WRRRYRRWRRRRRQRRRPRR-amide), and Q670-vCPP2319 (Quasar® 670-WRRRYRRWRRRRRQRRRPRR-amide) were synthesized in a Prelude instrument (Gyros Protein Technologies, Tuczon, Az, USA) running Fmoc solid phase synthesis protocols at 0.1 mmol scale on a Fmoc-Rink-amide ChemMatrix resin. Side chain functionalities were protected with *tert*-butyl (Tyr), trityl (Gln), N^G-2,2,4,6,7-pentamethyldihydrobenzofuran-5-sulfonyl (Arg), and *tert*-butoxycarbonyl (Trp) groups. Eight-fold excess of amino acids and HBTU, in the presence of double molar amount of DIEA, were used for coupling, with DMF as solvent. After chain assembly, full deprotection and cleavage were carried out with 95:2.5:2.5 (% v/v) TFA:H_2O:TIS for 90 min, at room temperature. The Q670-vCPP2319 peptide was similarly synthesized, except that Quasar® 670 (Q670) was coupled manually in a 4-fold molar excess with DIPCDI (4-fold molar excess) in DMF to the deprotected N-terminus prior to full deprotection and cleavage. Peptides were isolated by precipitation with cold diethyl ether and centrifugation at 4000 g, 4 °C for 20 min, taken up in H_2O and lyophilized.

Analytical reversed-phase high-performance liquid chromatography (RP-HPLC) was performed on a Luna C18 column (4.6 mm × 50 mm, 3 μm) (Phenomenex, USA). Linear gradients of solvent B (0.036 % TFA in acetonitrile) into solvent A (0.045 % TFA in H_2O) were used at a flow rate of 1 mL min^{-1} and with UV detection at 220 nm. Preparative HPLC runs were performed on a Luna C18 column (21.2 mm × 250 mm, 10 μm) (Phenomenex) using linear gradients of solvent B (0.1 % TFA in acetonitrile) into solvent A (0.1 % TFA in H_2O) at a flow rate of 25 mL min^{-1} and with UV detection at 220 nm. Fractions of adequate homogeneity and with the expected mass were combined and lyophilized. LC-MS was performed in a LC-MS 2010 EV instrument (Shimadzu, Kyoto, Japan) fitted with an Xbridge C18 column (4.6 mm × 150 mm, 3.5 μm) (Waters, Cerdanyola del Valles, Spain), eluting with linear gradients of formic acid/acetonitrile (0.08 % v/v) into formic acid/H_2O (0.1 % v/v) over 15 min at 1 mL min^{-1}. Peptide stock solutions (0.5 or 1 mM) in PBS were stored at −20 °C.

2.3. Cell culture

Human breast cell lines MDA-MB-231 (ATCC® HTB-26™), MCF 10A (ATCC® CRL-10317™) and cerebral microvascular endothelial cell line HBEC-5i (ATCC® CRL-3245™) were purchased from American Type Culture Collection (ATCC). MDA-MB-231 breast adenocarcinoma cells were cultured as a monolayer in DMEM supplemented with 10 % FBS and 1 % penicillin-streptomycin. MCF 10A breast cells were cultured as a monolayer in MEBM supplemented with SingleQuots, cholera toxin 100 ng/mL and 1 % penicillin-streptomycin, according to ATCC instructions. HBEC-5i cells were cultured on 0.1 % gelatin-coated T-flasks in DMEM:F12 medium as a monolayer. The medium was supplemented with 10 % FBS, 1 % penicillin/streptomycin, and 40 μg/mL endothelial growth supplement (ECGS), according to manufacturer's instructions. All cell cultures were maintained at 37 °C and 5 % CO_2 in a humidified atmosphere, with the medium changed every other day.

2.4. EVs isolation from human breast cells

MDA-MB-231 cell cultures with confluence over 80 % were washed with PBS and exosome-depleted media (DMEM with 10 % dFBS and 1 % penicillin-streptomycin) was added to the flasks. After 24–30 h, the media was collected and EVs were isolated using Total exosome isolation (from cell culture media) reagent, following the manufacturers' instructions. Briefly, the media was centrifuged at 2000 g, for 30 min at room temperature. The supernatant was collected, mixed with 0.5 vol of Total exosome isolation (from cell culture media) reagent and allowed to incubate overnight, at 4 °C. The samples were then centrifuged at 10 000 g, for 1 h at 4 °C. Finally, the supernatant was discarded, and the pellet was resuspended in PBS. MCF 10A cell cultures with confluence over 80 % had the media changed for fresh media and EVs were collected after 48 h, as described above. Protein concentration of the samples was determined using a Micro BCA™ protein assay kit, according to manufacturer's instructions. A calibration curve was prepared every time using a standard bovine serum albumin (BSA) solution and EVs samples were diluted before adding the working reagent. Absorbances were measured in a microplate reader Tecan Infinite® F500 (Männedorf, Zurich, Switzerland), at 570 nm.

2.5. EVs characterization by transmission electron microscopy (TEM)

TEM observations were performed on a Hitachi H-7000 instrument at an acceleration voltage of 100 kV, acquisitions and

measurements were performed using Megaview III side mount camera and iTEM software (Olympus®). To prepare the TEM samples, 5 μL of aqueous MDA-MB-231-derived EVs (EVs-MDA) or MCF 10A-derived EVs (EVs-MCF) were deposited onto a formvar (Agar Scientific®)/carbon-coated 400 mesh copper grid (Agar Scientific®). After 5 min the grid was washed in pure water and negatively stained with 2 % (w/v) aqueous Uranyl Acetate (Agar Scientific®) for approximately 2 min. The copper grid was air-dried prior to visualization.

2.6. EVs characterization by flow cytometry

The labelling of the EVs with the carboxyfluorescein succinimidyl ester (CFSE) dye was achieved by incubating the cells with the dye. Briefly, MDA-MB-231 or MCF 10A cells were harvested and concentrated to 20.0×10^6 cell/mL in Dulbecco's phosphate-buffered saline (DPBS). The cells were incubated with 100 μM CFSE in a water bath at 37 °C, for 15 min and then diluted 10 times. Labelled MDA-MB-231 and MCF 10A cells were centrifuged at 1250 and 1000 rpm, respectively, at room temperature for 5 min, resuspended in complete media, seeded, and allow to grow until EVs isolation, as described above. 100 μL of fresh samples with or without CFSE label were incubated with Alexa Fluor® 647 Mouse anti-Human CD63, PerCP-Cy™ 5.5 Mouse anti-Human CD105 and anti-EpCAM PE for 20 min at room temperature, with orbital agitation. An isotype control was performed using PE Mouse IgG1, κ Isotype Control. After the incubation all the samples were diluted by adding 1 mL of PBS.

Flow cytometry was performed on a BD LSRFortessa (BD) using FACSDiva 6.2 software. The detection threshold was set in the FITC channel to 200 nm. For size calibration, 100 nm nanobeads with inherent fluorescence detectable through the FITC channel were used. All samples were analyzed using the same voltage settings. Data was processed with FlowJo version 10.3. After correction for auto-fluorescence, CD63, CD105 and EpCAM expression, as well as the presence of intraluminal CFSE were presented as fluorescence arbitrary units and positive events.

2.7. Zeta potential measurements

EVs-MDA and EVs-MCF were diluted in PBS buffer. Samples of EVs with and without the peptide were prepared and loaded into disposable zeta cells with gold electrodes and allowed to equilibrate for 15 min at 37 °C. Each experiment consisted in a set of 15 measurements with automatically defined number of subruns (ranging from 10 to 100) performed on the Malvern Zetasizer Nano ZS (Malvern, UK), at a constant voltage of 40 V. The complete experiment was carried out at least two times using independent EVs samples and a control (EVs without peptide) was performed in each day.

2.8. Surface plasmon resonance (SPR) with EVs-MDA, EVs-MCF and vCPP2319

SPR experiments were performed in a Biacore ×100 (GE Healthcare). PBS was used as running buffer and temperature was set at 37 °C for all experiments. The L1 sensor chip was used for all experiments. Previously to each experiment, the flow system was primed three times and the sensor chip surface was washed with three injections of 20 mM CHAPS. EVs were deposited in the L1 sensor chip for 2400 s, at 2 μL/min flow rate. Loose EVs were removed by injecting 10 mM NaOH at 50 μL/min. A stabilization period of 2400 s was set to evaluate the stability of the deposited EVs' layer. The protein concentration of the EVs samples ranged from 1 to 200 μg/mL for EVs-MDA and 1–75 μg/mL for EVs-MCF. vCPP2319 was injected over the pre-formed layer of EVs with a contact time of 250 s, at 5 μL/min, and allowed to dissociate for 800 s. The L1 sensor chip was regenerated after 3 cicles of 10 alternated injections of 80 mM gluco-pyranoside (5 μL/min, 60 s) and 0.5 % (w/v) SDS (5 μL/min, 60 s) followed by one injection of 20 mM CHAPS (5 μL/min for 60 s) and one injection of 10 mM NaOH containing 20 % (v/v) methanol (50 μL/min for 36 s). Baselines response values were compared before and after each measurement to assure surface regeneration effectiveness. SPR sensorgrams were collected for EVs deposition, vCPP2319 binding to the deposited layer of EVs and vCPP2319 injection in an L1 chip without previously deposited EVs. EVs deposition response was collected from the sensorgram after reaching a stable response. For the study of the interaction between EVs and vCPP2319, the dissociation data was collected from 250 to 1050s of each sensorgram.

2.9. Cellular proliferation assay

2.9.1. MDA-MB-231 and MCF 10A human breast cells

An MTT assay was used to evaluate the cytotoxic activity of vCPP2319 combined with EVs-MDA towards breast cell lines MDA-MB-231 and MCF 10A, as previously described [34]. Briefly, MDA-MB-231 and MCF 10A cells were seeded at 3.0×10^4 cells/mL and 5.0×10^5 cell/mL, respectively, into a 96-well plate, with a volume of 100 μL/well, and incubated for 24 h. After media removal, cells were washed once with PBS and complete serum-free media with different EVs protein concentrations was added to cells followed by vCPP2319 in the selected concentration (5.2, 18.2 or 20 μM), in a final volume of 100 μL/well. The EVs protein concentrations ranged between 1 and 100 μg/mL. Following a period of incubation of 24 h, 10 μL of a 5 mg/mL solution of MTT was added to each well and allowed to incubate for 2 h. Finally, content was removed from each well, and 150 μL of spectrophotometric grade DMSO was added to each well, to dissolve the resulting formazan crystals. Absorbance was measured at 540 nm in a microplate reader Tecan Infinite® F500.

Positive control (100 % cell viability) was performed adding serum-free medium to the cells (untreated cells). Negative controls (0 % cell viability) were performed adding serum-free medium with 20 % and 30 % DMSO to MDA-MB-231 and MCF 10A cells, respectively. Cell viability (%) was determined as:

$$\frac{\text{Absorbance}_{\text{treated cells}}}{\text{Absorbance}_{\text{untreated cells}}} \times 100,$$

and cell death was assessed as follows:

$$\text{Cell death (\%)} = 100 - \text{Cell viability (\%)}.$$

IC$_{50}$ values were assessed using GraphPad Prism 6.0 software package using log (inhibitor) vs. normalized response. The experiments were performed in different days with independently grown cell cultures.

2.9.2. HBEC-5i human brain endothelial cells

The cytotoxicity of vCPP2319 combined with EVs-MDA was determined using CellTiter-Blue® cell viability assay following a protocol previously optimized [35]. Briefly, cells were allowed to grow until 80 % confluence in a culture T-flask. Then, they were carefully harvested with trypsin-EDTA and seeded at 1.0×10^4 cells/well into pre-coated with attachment factor protein solution 96-well clear flat-bottomed polystyrene plates (Corning, USA) for 24 h. Subsequently, they were washed two times with $1 \times$ PBS and one time with DMEM:F12 medium, and 100 μL of previously diluted EVs-MDA samples, ranging from 1.0 to 100.0 μg/mL, with or without vCPP2319 5.2 μM in DMEM:F12 medium, were added to cells. After 24 h, cells were washed two times with $1 \times$ PBS and one time with DMEM:F12 medium and 20 μL of CellTiter-Blue® Reagent (diluted in 100 μL of DMEM:F12 medium) was added to each well and incubated for 3 h in culturing conditions.

Fluorescence ($\lambda_{ex} = 560$ nm, $\lambda_{em} = 590$ nm), was measured in a Thermo Fischer Varioskan^{TM} LUX multimode microplate reader. Complete medium and medium containing 0.25 % Triton X-100 were used as positive and negative controls (100 and 0 % viability), respectively. Cell viability (%) was determined as:

$$\text{Cell Viability (\%)} = \frac{F_{\text{treated}} - F_{\text{blank}}}{F_{\text{untreated}} - F_{\text{blank}}} \times 100$$

where F_{treated} is the fluorescence intensity of treated cells, $F_{\text{non treated}}$ is the fluorescence of untreated cells and F_{blank} is the fluorescence of CellTiter-Blue® reagent in complete medium without cells. Experiments were performed in triplicates on different days using three independently grown cell cultures.

2.10. In vitro BBB translocation assay

The translocation ability of all samples was assessed using an *in vitro* BBB model previously optimized using HBEC-5i cell line [35]. Briefly, cells were allowed to grow until 80 % confluence in a culture T-flask. Then, they were carefully harvested with trypsin-EDTA and seeded at 8.0×10^3 cells/well into tissue culture inserts (transparent polyester (PET) membrane with 1.0 μm pores) for 24-well plates (BD Falcon, USA) pre-coated with attachment factor protein solution. The medium was changed every other day for 8 days, and, afterwards, cells were washed two times with $1 \times$ PBS and one time with DMEM:F12 without phenol red. Next, samples were prepared in DMEM without phenol red, at a final concentrations of 1 μg/mL CFSE labelled EVs-MDA and/or 5.2 μM of Q670-vCPP2319 and incubated for 1 h at 37 °C and 200 rpm, protected from the light. The samples were then added to the apical side of the *in vitro* BBB model and incubated for 24 h. Finally, samples from the apical and basolateral side were collected and fluorescence intensity of the samples, at $\lambda_{ex} = 492$ nm, $\lambda_{em} = 517$ nm (λ492/517) for EVs-MDA or $\lambda_{ex} = 647$ nm, $\lambda_{em} = 666$ nm (λ647/666) for vCPP2319 was measured.

EVs-MDA and vCPP2319 translocation was determined by fluorescence intensity (λ492/517 and λ647/666, respectively), using a Thermo Fischer Varioskan^{TM} LUX multimode microplate reader. The percentage of EVs, vCPP2319 or EVs + vCPP2319 that translocated the *in vitro* BBB model was obtained as samples recovery (%), being calculated as follows:

$$\text{Recovery (\%)} = \frac{F_i - F_{\text{cells}}}{F_{\text{sample}} - F_{\text{Medium}}} \times 100$$

where, F_i is the fluorescence intensity of samples recovered, F_{cells} is the intrinsic fluorescence intensity of cells without samples incubation, F_{sample} is the intensity of total sample initially added to the transwell apical side, and F_{Medium} is the intensity of DMEM:F12 medium without phenol red. Experiments were performed in triplicates on different days using three independently grown cell cultures.

2.11. In vitro BBB integrity assay

After the *in vitro* BBB translocation assay, cells were washed two times with $1 \times$ PBS and one time with DMEM:F12 medium without phenol red, and integrity of the barrier evaluated using tetramethylrhodamine isothiocyanate-4 kDa dextran (RD4) (Sigma-Aldrich, Spain), previously diluted in DMEM:F12 medium without phenol red to an absorbance below 0.1, for 2 h. Samples were collected from the apical and basolateral side and fluorescence intensity measured at $\lambda_{ex} = 550$ nm, $\lambda_{em} = 577$ nm using a Thermo Fischer Varioskan^{TM} LUX multimode microplate reader. The RD4 Permeability (%) was determined using the following equation:

$$\text{RD4 Permeability}(\%) = \frac{F_i\text{-}F_{cells}}{F_{RD4}\text{-}F_{Medium}} \times 100$$

where: F_i is the fluorescence intensity of samples recovered, F_{cells} is the intrinsic fluorescence intensity of cells without samples incubation, F_{RD4} is the intensity of total RD4 initially added to the transwell apical side, and F_{Medium} is the intensity of DMEM:F12 medium without phenol red.

The integrity of the barrier is indirectly proportional to the percentage of RD4 recovered and was determined using the following equation:

$$\text{Recovery } (\%) = 100\text{-RD4 Permeability } (\%)$$

Experiments were performed in triplicates on different days using three independently grown cell cultures.

3. Results and discussion

EVs refer to a broad population of vesicles, secreted by virtually all cells, that constitute a communication system that has been intensively studied, throwing new light into cell-to-cell communication and raising new perspectives for medical advance [16,36]. According to the latest position statement by the International Society for Extracellular Vesicles (ISEV), consensus on specific markers for EV subtypes, i.e., exosomes and MVs, specifically linking an EV to a specified biogenesis pathway, is yet to be achieved [37].
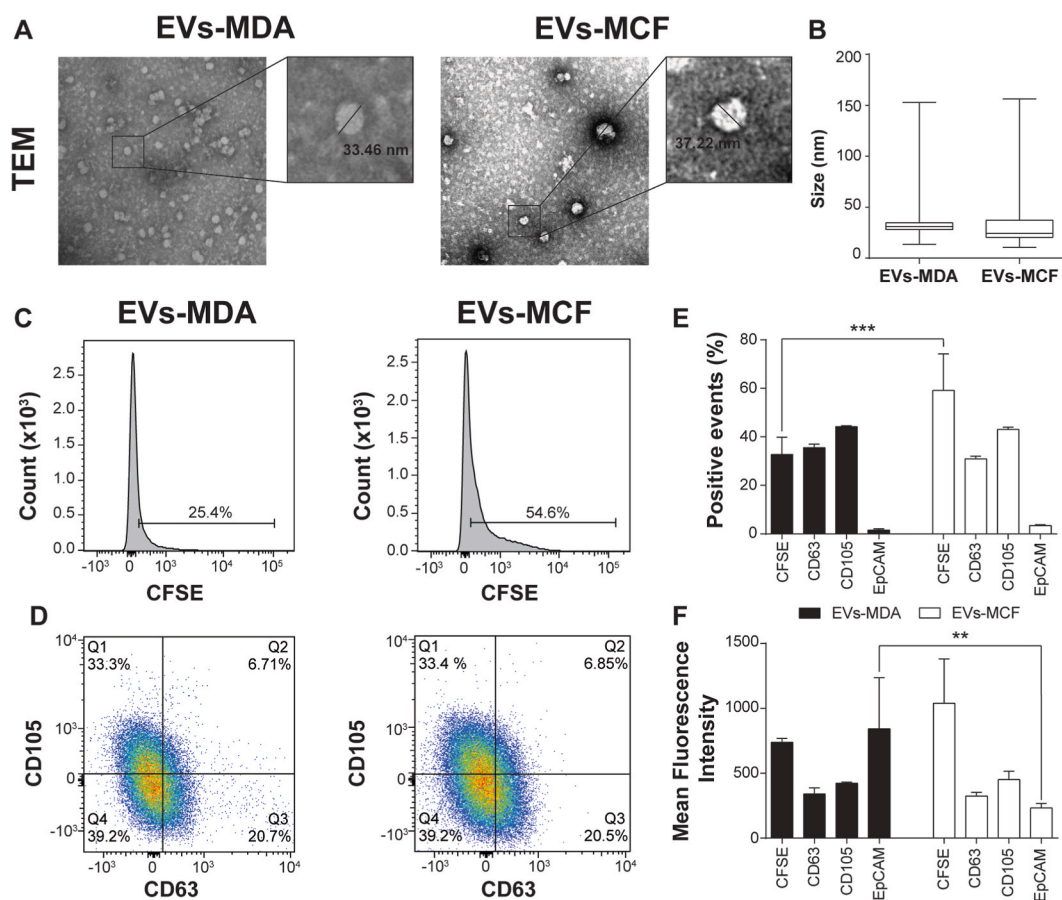

Fig. 1. TEM imaging of extracellular vesicles (EVs) isolated from MDA-MB-231 and MCF 10A cell cultures (EVs-MDA and EVs-MCF, respectively) and molecular characterization by flow cytometry. EVs were isolated from MDA-MB-231 and MCF 10A cell cultures using the Total Exosome Isolation reagent (Invitrogen) and samples were imaged by TEM (A). The displayed images were proportionally resized from raw images with an 100 000 × magnification. The sizes of the vesicles, obtained by measuring the diameter of the vesicles in raw TEM images, are also shown (B). Five independent samples were analyzed through TEM for EVs-MDA and EVs-MCF in at least 3 different days. Significance was assessed by unpaired *t*-test and no significant differences were detected between the sizes of the EVs from both cell types. The EVs were also characterized by flow cytometry (C to F). CFSE was added to the cells in culture, and it was used as an intraluminal dye. The presence of CD63, CD105 and EpCAM at the surface of the vesicles was studied. Relative frequency of CFSE (C) and CD105 vs CD63 (D) are shown for EVs-MDA and EVs-MCF. Positive events (%) (E) and mean fluorescence intensity (MFI) (F) are shown for each marker. Flow cytometry characterization was repeated in three different days, with independent samples, for each type of EVs. Significance was assessed by ANOVA followed by Tukey's post-test. ** p-value ≤0.01, *** p-value ≤0.001.

Therefore, in this work we will be using the term "extracellular vesicles" (EVs) to refer to lipid bilayer particles without a functional nucleus, naturally released from cells [37].

3.1. Characterization of breast cells' EVs

EVs were isolated from culture media of MDA-MB-231 and MCF 10A cell cultures using Total Exosome Isolation reagent (Invitrogen). The obtained samples were characterized by transmission electron microscopy (TEM) and flow cytometry (Fig. 1). TEM images (Fig. 1 – **A**) from MDA-MB-231 EV samples (henceforth EVs-MDA) and MCF 10A EVs (henceforth EVs-MCF) revealed small round vesicles with occasional formation of clusters that suggest a tendency to aggregate. Exosome aggregation has been described before and its extent may vary with the isolation method used and the sample concentration [38–40]. EVs-MDA and EVs-MCF had mean diameters of 33.2 ± 12.5 and 34.0 ± 25.1 nm, respectively, ranging from ca. 15–150 nm in both cases (Fig. 1 – B). These results are in line with other EV characterizations by TEM [41,42]. EVs-MDA and EVs-MCF were also characterized by atomic force microscopy (AFM), with results again in line with those from other studies [43].

To further characterize EVs-MDA and EVs-MCF from a molecular point of view, we used flow cytometry to detect CFSE and the presence of EpCAM, CD63 and CD105, previously used as EV markers [44–52] (Fig. 1 – C to F). The results show a significant difference in the number of CFSE-positive events for EVs-MCF vs. EVs-MDA, suggesting more extensive CFSE-labeling of EVs from MCF 10A than of those from MDA-MB-231 cells (Fig. 1 – C and E). The CFSE dye was added to the cells in culture and then detected within the lumen of the EVs isolated from the cell culture media. This observation supports the presence of biological vesicular particles obtained from the cell cultures [45]. As an intracellular dye, the CFSE signal will proportionally decrease each time the cells divide [53]. MDA-MB-231 are highly proliferative and invasive TNBC cells [54,55]. In agreement, the protein concentration of samples with EVs-MDA was consistently higher when compared to EVs-MCF (data not shown), which also agrees with previous studies showing that cancer cells release high amounts of EVs and cancer patients have higher levels of exosomes in their blood [56–58]. Therefore, it is not surprising to find fewer EVs-MDA with CFSE labelling and lower mean fluorescence intensity (MFI) values, since CFSE will be
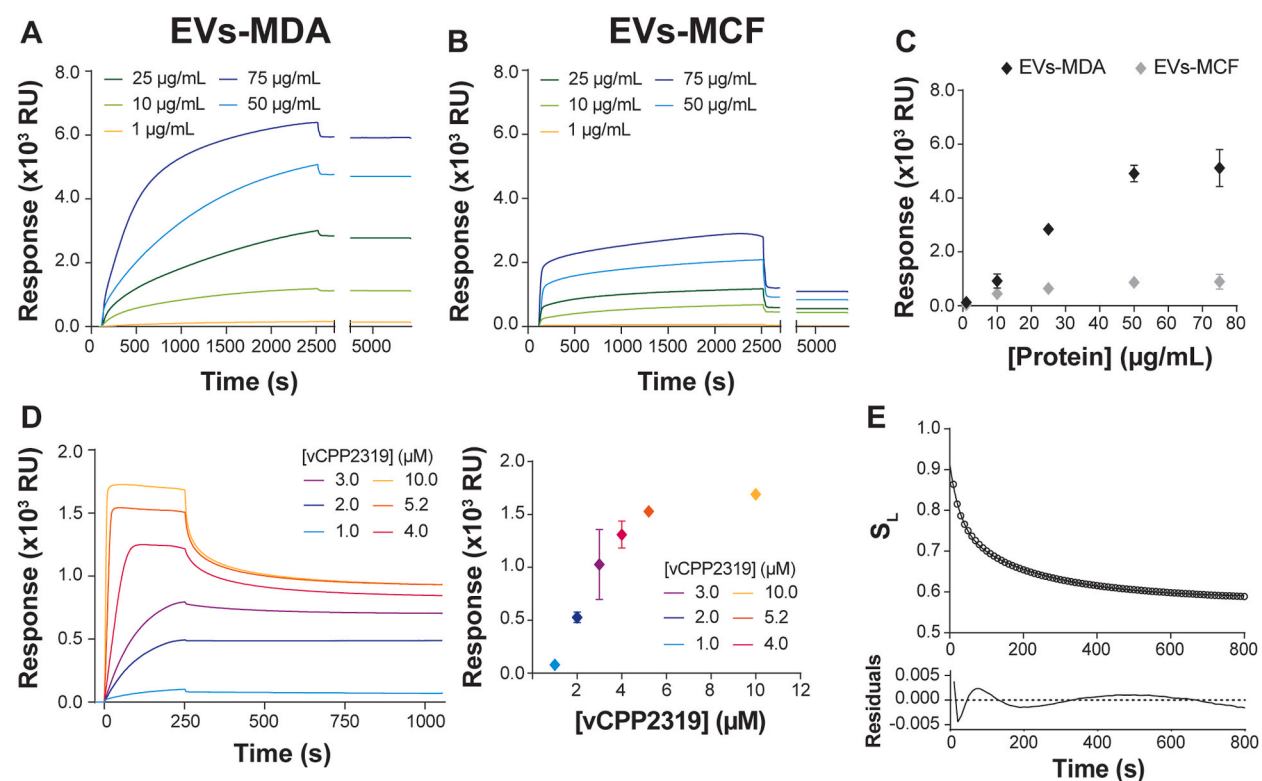

Fig. 2. Study of the interaction between vCPP2319 and extracellular vesicles derived from MDA-MB-231 through surface plasmon resonance (SPR). EVs isolated from MDA-MB-231 (EVs-MDA) and MCF 10A cells (EVs-MCF) were injected at several protein concentrations ranging from 1 to 75 μg/mL over an L1 sensor chip and the sensorgrams were recorded (A and B). A comparison of the response between the EVs origin was obtained by plotting the final response values for each protein concentration (C). Several vCPP2319 concentrations ranging from 1.0 to 10.0 μM were injected on EVs-MDA deposited over the L1 sensor chip at a concentration of 75 μg/mL, sensorgrams were recorded and the final response values were plotted as function of the peptide concentration (D). A dissociation analysis was performed, and the peptide fraction associated to the deposited EVs (S_L) was plotted as a function of the dissociation time. The curve represents the two-phase decay fit to the data and the respective residual plots are represented. The sensorgrams in A, B and D and the dissociation analysis in E are representative replicates. Error bars in C and D correspond to the standard error of independent replicates. All experiments were performed in duplicate (n = 2).

distributed throughout the cells in culture and the EVs released by these cells (Fig. 1 – E and F). Another significant difference was obtained for the MFI values of EpCAM in EVs-MDA and EVs-MCF (Fig. 1 – F), even though the presence of this marker was not significantly detected above the isotype control background. Nonetheless, despite the presence of EVs with EpCAM being very low in samples from both cell lines, EVs-MDA had higher levels of EpCAM when compared with EVs-MCF. EpCAM is a membrane protein that is often overexpressed in tumors and is recruited to exosomes, therefore it has been reported as a molecular marker for TDEs [59]. This result is in line with other studies displaying high levels of EpCAM for EVs-MDA [60]. The majority (around 60 %) of the EVs had CD63, CD105 or both surface markers (Fig. 1 – D). CD63 (also known as TSPAN30) is a tetraspanin widely used as an exosomal marker and it is involved in exosomes' biogenesis [47,49,61–63]. CD105 (also known as endoglin) is a transmembrane glycoprotein involved in angiogenesis and its overexpression has been associated with tumor cell migration and intravasation via endothelium destabilization [50–52]. In a recent study, CD105 was identified as an EV protein adequate to be used as biomarker for MBC in EVs samples obtained from patients using a commercial kit [50]. Moreover, CD105+ EVs obtained from renal cancer stem cells were shown to participate in the lung metastization process, which is also a favorable metastatic site in MBC [6,64]. Therefore, CD105 was used as a biomarker for MBC-derived EVs, which was linked with the metastization process [50,64]. Interestingly, no significant differences between the presence of CD63 and CD105 in EVs-MDA and EVs-MCF were observed.

Overall, considering the results obtained from TEM imaging and flow cytometry, we conclude that the NPs obtained from MDA-MB-231 and MCF 10A cells have sizes and surface proteins consistent with EVs that can potentially contribute to the development of an efficient DDS. Hence, we decided to study the interaction between these EVs and vCPP2319.

3.2. Interaction between vCPP2319 and breast cells' EVs

The binding of vCPP2319 to EVs-MDA and EVs-MCF was investigated using two biophysical techniques: surface plasmon resonance
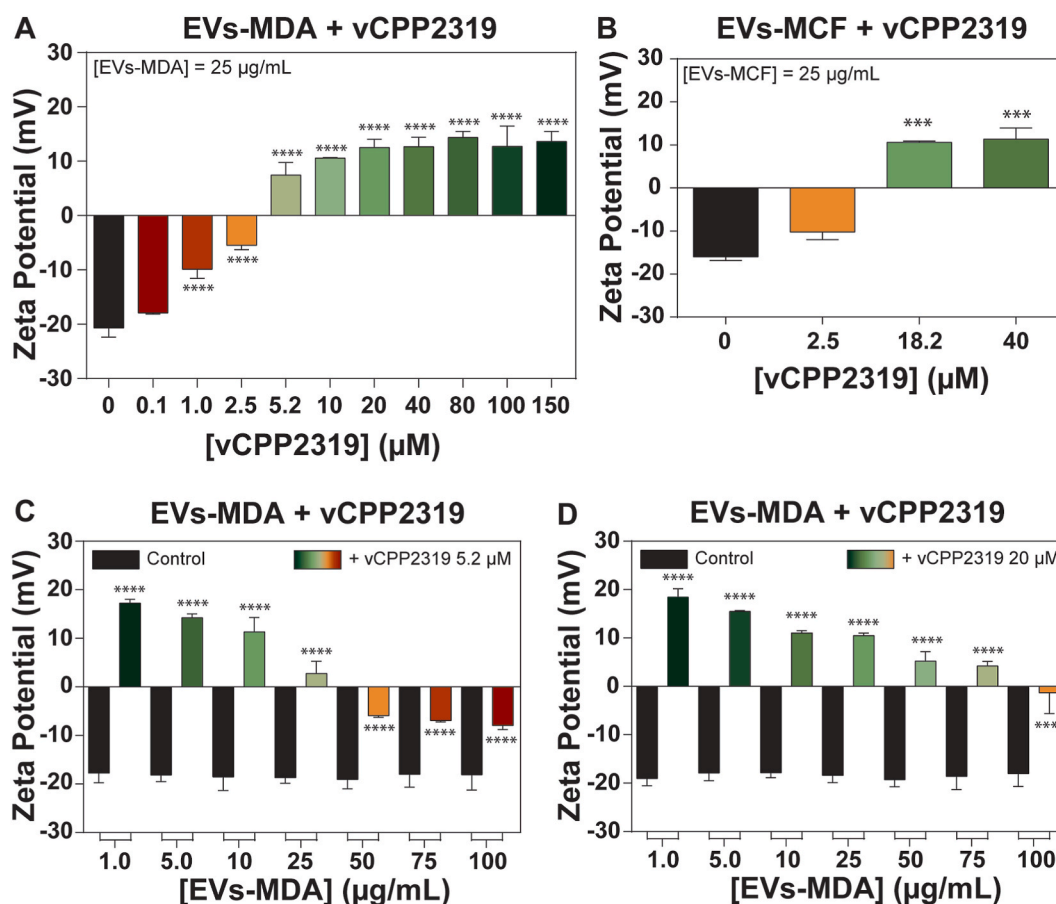

Fig. 3. Study of the interaction of vCPP2319 with extracellular vesicles isolated from breast cells through zeta potential. Zeta potential measurements were performed with EVs obtained from MDA-MB-231 (EVs-MDA) (A) and MCF 10A cells (EVs-MCF) (B) in the absence (n = 5 and n = 2, respectively) and presence of vCPP2319, at increasing peptide concentrations (n = 2). The zeta potential of EVs-MDA was also measured in the absence and presence of vCPP2319 at fixed concentrations of 5.2 (C, n = 3) and 20 μM (D, n = 2), in a range of protein concentration for EVs-MDA samples of 1–100 μg/mL. Error bars refer to the standard deviation. Significance was assessed by ANOVA followed by Sidak's post-test. ***P-value ≤0.001; ****P-value ≤0.0001.

(SPR) (Fig. 2) and dynamic light scattering (DLS), namely zeta potential (Fig. 3). In these studies, EVs concentration will be taken implicitly from the EV-associated protein concentrations, as determined using a Micro BCA protein assay kit.

Two different experimental set ups were considered for the SPR experiments. In a first run, EVs samples with different protein concentrations were injected over the L1 sensor chip to evaluate deposition and establish an optimal concentration (Fig. 2 – A to C). Next, EVs at the optimal concentration were injected over the L1 sensor chip to ensure a saturated surface. Then, after a stable sensorgram baseline was achieved, vCPP2319 was injected (Fig. 2 – D and E). For EVs immobilization, the commonly used procedure for liposome deposition on L1, previously validated in our lab [62], was followed [65–67]. In this method, EVs bind to the hydrophobic L1 surface, composed of alkyl groups covalently bound to a carboxymethylated dextran matrix [65,66]. The EVs-MDA gradually covered the dextran matrix to form a stable surface that was maintained after sample injection interruption (around 2500 s) and NaOH wash (which occurs within the gaps represented in the sensorgrams); (Fig. 2 – A). With EVs-MCF, a different behavior, with much lower increase in response over time was observed, becoming almost undetectable after injection interruption (around 2500 s), and suggesting rather poor EV deposition (Fig. 2 – B). Moreover, both EVs types have different impact on responses to concentration: while EVs-MDA show increased final baseline response with concentration, EVs-MCF do not show such effect (Fig. 2 – C). This difference suggests that EVs-MDA and EVs-MCF have different molecular compositions [68,69]. The fact that not only EVs-MCF covers the L1 sensor surface deficiently but also that vCPP2319 binds strongly to the naked L1 surface (Figs. S1–A) makes the study of the interaction between vCPP2319 and EVs-MCF by SPR unfeasible (Figs. S1–B).

L1 sensor chip saturation by EVs-MDA was observed by increasing protein concentration up to 200 μg/mL (Figs. S1–C). For concentrations above 75 μg/mL the increase in response was not significant, therefore this concentration was selected. vCPP2319 was flown over EVs-MDA on the L1 chip, and the sensorgrams are shown in Fig. 2 – D. The response increased with vCPP2319 concentration until saturation at 5.2 μM. Interestingly, for 5.2 and 10 μM peptide, a sharp increase in the response right after injection (time 0) was observed, followed by a plateau until injection was interrupted (250 s). For concentrations below 5.2 μM, the increase in response was slower, with a smaller and shorter plateau at 4 μM, and no plateau for 1–3 μM vCPP2319. Moreover, after the plateaus at 5.2 and 10 μM vCPP2319, a fast, short drop in response is observed after interrupting peptide injection, followed by stabilization until the end of the sensorgram. This dissociation profile suggests that, upon interrupting vCPP2319 flow, a fraction of the peptide interacting with immobilized EVs-MDA is flushed out while another fraction (S_L) is retained and can be assessed by the dissociation model of Figueira et al. [65] (Fig. 2 – E). This analysis revealed that S_L variation during dissociation fits well with a two-phase decay profile, with a final S_L value around 0.6, suggesting that approximately 40 % of vCPP2319 molecules establish a transient interaction with the EVs-MDA surface that is lost when peptide injection stops, and approximately 60 % that remains bound even when vCPP2319 input is interrupted, a sufficiently large fraction to warrant the use of EVs-MDA as potential DDS for vCPP2319.

It is worth mentioning that, in most published works using SPR to characterize EVs, the deposition is done on a pre-functionalized sensor chip surface, a time-consuming process requiring additional reagents [69–74]. In contrast, in this work direct EVs immobilization with no supplementary chemicals has been applied. To our best knowledge, this is the first case where such approach has been used in SPR experiments (with EVs from two different cell lines and applying a dissociation model). To note, Thakur et al. investigated direct EVs interaction with either antibody-functionalized or naked sensor chips using localized SPR and were able to detect interaction in a concentration-dependent manner [69]. Overall, these results support the use of the SPR as a versatile technique to study peptide-membrane interactions using EVs other than liposomes.

Considering the ability of EVs-MDA to bind vCPP2319, we hypothesized that direct incubation would suffice to assemble EVs-vCPP2319 nanoparticles, as previously used for other drugs such as doxorubicin, curcumin or paclitaxel [36,75–78]. To further explore the peptide-EV interaction and establish optimal conditions, we performed zeta potential measurements (Fig. 3). Results show that EVs have a negative net surface charge, as previously described [62,63,79–84]. We also confirmed that the zeta potential for EVs-MDA (−20.7 ± 1.72 mV) is lower than that for EVs-MCF (−16.0 ± 0.82 mV), as found in another study [84]. Importantly, this result supports the potential use of EVs in DDS since a considerable negative surface charge may contribute to improve stability and dispersibility in body fluids, therefore increasing the translatability to target tissues [82]. As the peptide concentration increases, there is an increase of the zeta potential value, which suggests an interaction between vCPP2319 and EVs-MDA (Fig. 3 – A). In both cases, there is a tendency for vCPP2319, which is cationic, to accumulate on the anionic surface of the EVs, leading to an increase of the zeta potential towards positive values, with an inversion of the overall surface charge of the EVs occurring between 2.5 and 5.2 μM for EVs-MDA. Curiously, 5.2 μM corresponds to the IC$_{50}$ we previously assessed for vCPP2319 towards MDA-MB-231 cells [30]. Moreover, the surface of EVs-MDA appears to get saturated at 20 μM of vCPP2319, since above this concentration there is no significant increase of the zeta potential values with the increase in peptide concentration. To further test the hypothesis that EVs neutralization correlates to cellular IC$_{50}$, we also tittered EVs-MCF with vCPP2319. Remarkably, neutralization occurred before 18.2 μM (Fig. 3 - B), the IC$_{50}$ obtained for MCF 10A cells [30]. Nonetheless, the correlation between the zeta potential values of EVs and their cells of origin has been addressed before [82,84]. This similarity may be explained by EVs biogenesis. Exosomes' biogenesis initiates with invaginations of the endosome and MVs result from the direct shedding of the plasma membrane [15,16,18,20–22]. Interestingly, in a previous study with vCPP2319 and MDA-MB-231 and MCF 10A cells, zeta potential measurements were performed at the same peptide concentrations and no significant changes were observed [30]. These results are deemed important because despite being in line with evidence showing a certain degree of similarity between the membrane of EVs and respective cells of origin, they are also evidence of critical differences that lead to opposite responses obtained for EVs and respective cells of origin when in the presence of vCPP2319 [30].

Aiming for an optimization of the loading of EVs with vCPP2319 we performed additional zeta potential measurements, this time titrating the peptide with EVs-MDA. Considering the results discussed above, we selected two peptide concentrations: 5.2 μM, the neutralization concentration in the previous titration, and 20 μM, the saturation concentration in the previous titration (Fig. 3 - C and D). As expected, the results show a decrease in the zeta potential towards negative values. The peptide:EVs ratio at which

neutralization occurs is consistent in Fig. 3 – A, C and D: approximately 0.1 μM peptide per μg/mL of EVs proteins, which corresponds to 1×10^{-4} mol of peptide per g of protein, or 0.32 g of peptide per g of protein, considering MW(vCPP2319) = 3179 g/mol. Saturation is achieved at 10-fold higher concentration of peptide, i.e.: 3.2 peptide:EVs protein mass ratio.

3.3. Cytotoxicity of vCPP2319 combined with TNBC EVs

To further explore the potential anticancer activity and selectivity of the previously identified combinations, we incubated breast cancer and healthy cells with EVs-MDA combined with 5.2 or 20 μM vCPP2319. This procedure was repeated with MCF 10A cells but 18.2 μM was used instead of 20 μM because it corresponds to the IC_{50} obtained for vCPP2319 towards this cell line [30]. The cytotoxic activity of the EVs-MDA with protein concentration ranging from 1 to 100 μg/mL, with or without vCPP2319, was evaluated through MTT assay (Fig. 4). In these experiments, the EVs and the peptide were added directly to the cells in the well, without being pre-incubated. The results show that EVs-MDA are slightly more toxic towards MCF 10A than MDA-MB-231 cells. Interestingly, by analyzing the results obtained with EVs-MDA and 5.2 μM vCPP2319 (Fig. 4 – **A and D**), we can clearly observe a different response for cells treated with EVs-MDA at protein concentrations below 20 μg/mL. For MDA-MB-231 cells (Fig. 4 – A) treated with EVs-MDA and 5.2 μM vCPP2319, the cell death increases with lower protein concentrations, while for MCF 10A cells, in the same conditions, (Fig. 4 – D), cell death decreases. Although this may seem like a promising effect, suggesting that the combination of EVs-MDA and vCPP2319 could result in a more potent and more selective cytotoxic activity of the peptide towards cancer cells, the results obtained for the cells treated with peptide alone show a very similar percentage of cell death (Fig. 4 – C and F). Therefore, the combination does not result in a more potent nor selective cytotoxic activity: the presence of EVs-MDA at 1 μg/mL does not impact peptide's activity at 5.2 μM towards MDA-MB-231 or MCF 10A cells. Similarly, for the highest peptide concentrations – 20 and 18.2 μM – we observe a constant percentage of cell death throughout the range of EVs-MDA protein concentration, suggesting that the presence of EVs-MDA did not impact on the peptide's activity at these concentrations (Fig. 4 – B and E). However, since the presence of EVs-MDA did not improve the selective cytotoxicity, we ruled out 18.2 μM when preparing an EVs-based DDS. Therefore, 5.2 μM was the peptide concentration selected to proceed, combined with EVs-MDA at 1 μg/mL. At this concentration, in the absence or presence of EVs-MDA it is possible to achieve a considerable percentage of cell death in MDA-MB-231 cells while sparing MCF 10A cells. Moreover, even though no significant advantage was obtained by using 5.2 μM vCPP2319 in combination with EVs-MDA at 1 μg/mL, there might be an advantage when using this system in terms of drug delivery. Therefore, the next step was to evaluate if the combination of EVs-MDA with vCPP2319 would allow for brain delivery.
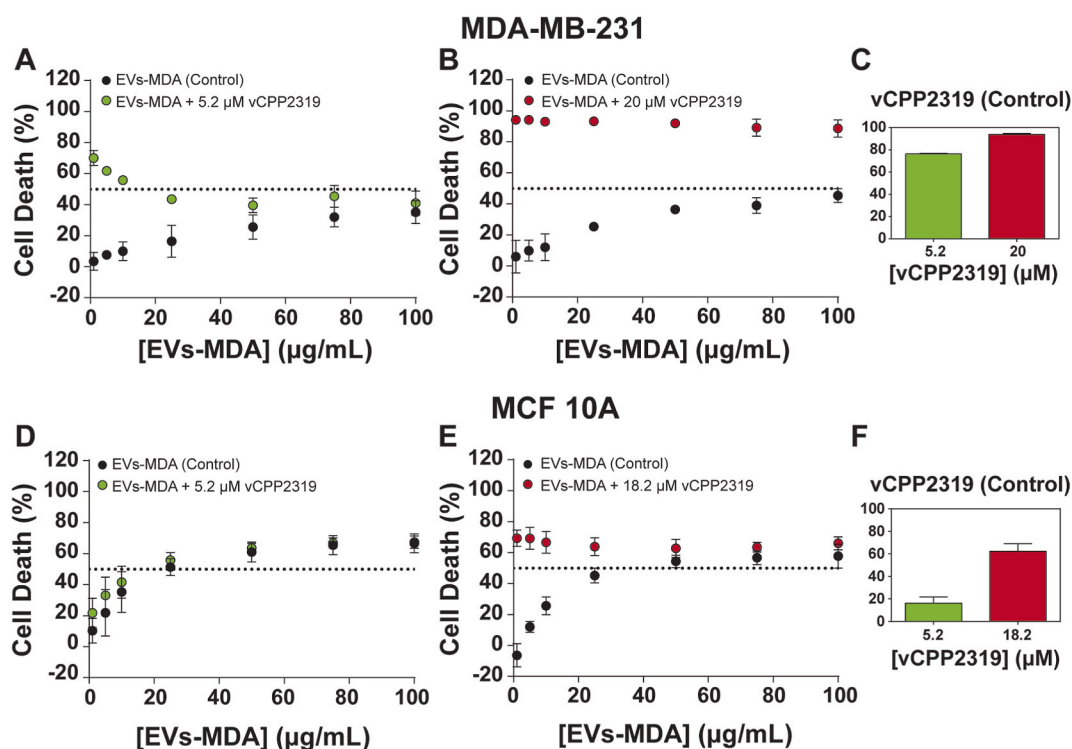

Fig. 4. Cytotoxic activity of breast cancer and healthy cells treated with vCPP2319 and breast cancer extracellular vesicles (EVs), added simultaneously to the well. MDA-MB-231 (A, B and C) and MCF 10A cells (D, E and F) were treated with vCPP2319 at the concentrations of 5.2 μM and 20 or 18.2 μM, in the presence (A, B, D and E) and absence (C and F) of EVs isolated from MDA-MB-231 (EVs-MDA), in concentrations ranging from 1 to 100 μg/mL. Error bars refer to the standard deviation. All experiments were performed in triplicate (n = 3).

3.4. *BBB translocation of vCPP2319 combined with TNBC EVs*

Amongst the several features that make EVs potential carriers, perhaps the most remarkable one is their natural ability to translocate biological barriers [85]. From all these barriers, the BBB has been the most extensively studied and it is also the most difficult challenge for a DDS [85]. In fact, 98 % of small drugs and practically 100 % of large drugs cannot cross the BBB [86]. Despite the classification of the EVs subclasses remaining a topic opened for debate, several studies show evidence which demonstrate the ability of exosomes to translocate through the BBB and deliver their cargo in the brain [22,75,85,87]. Therefore, the final step of this study was to evaluate if EVs-MDA could carry vCPP2319 through an *in vitro* BBB model.
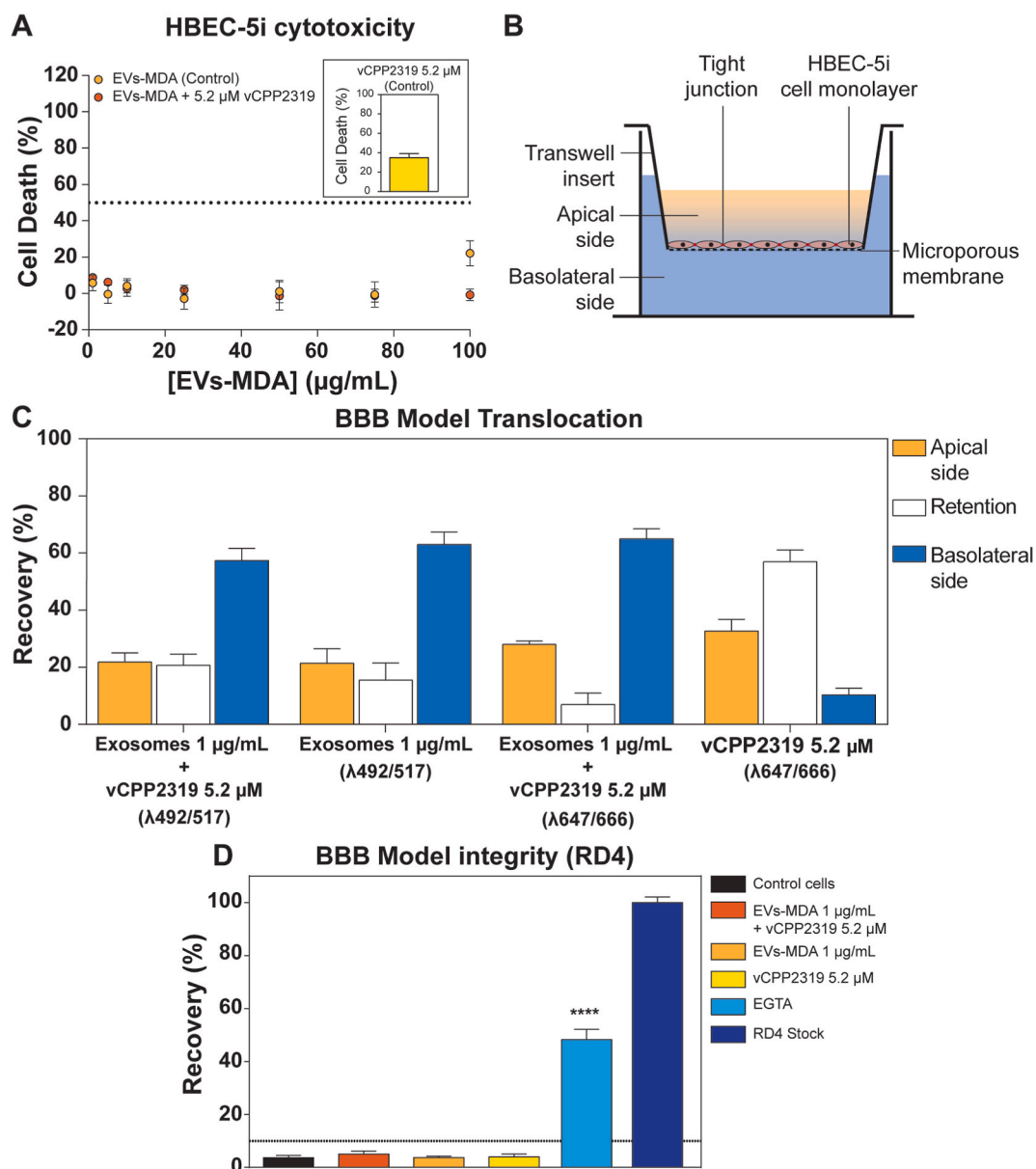

Fig. 5. Translocation of an *in vitro* monoculture BBB model by extracellular vesicles isolated from MDA-MB-231 cells (EVs-MDA) combined with 5.2 µM vCPP2319. The cytotoxic activity of EVs-MDA (1–100 µg/mL) towards human brain endothelial cells HBEC-5i was evaluated, with and without vCPP2319 5.2 µM (A). A scheme of the experimental setup of the BBB model is shown (B): HBEC-5i are cultured as monolayer on the apical side of a polyester (PET) transwell insert with 1.0 µm pore size. The BBB model translocation by the EVs-MDA, vCPP2319 and the combination of both was then evaluated by adding them at the apical side and measuring their presence on the apical and basolateral side after 24 h (D). EVs-MDA were labelled with CFSE and vCPP2319 was labelled with Quasar® 670 to allow for fluorescent detection. Error bars refer to standard deviation. These experiments were performed with independently grown cultures in three different days. Significance was assessed by two-way ANOVA followed by Tukey's post-test (C) and one-way ANOVA followed by Dunnett's post-test (D). ****P-value ≤0.0001.

First, the cytotoxicity of EVs-MDA with protein concentration ranging from 1 to 100 μg/mL was studied towards HBEC-5i, in the presence or absence of vCPP2319 at 5.2 μM, and no significant effects were observed (Fig. 5 – A). Therefore, since EVs-MDA, vCPP2319 or their combination did not reveal any significant cytotoxicity towards HBEC-5i we are able to use these cells in a BBB *in vitro* monoculture model. EVs-MDA labelled with CFSE were incubated with vCPP2319 labelled with Quasar® 670 for 1 h and then added to the apical side of a transwell (Fig. 5 – B). After 24 h, the samples were collected from both the apical and the basolateral side and the presence of EVs-MDA-CFSE (λ492/517) or vCPP2319-Q670 (λ647/666) was detected by measuring the fluorescence intensity of the samples. The results (Fig. 5 – C) show a very similar percentage of EVs-MDA (λ492/517) in the basolateral and apical side for EVs-MDA 1 μg/mL + vCPP2319 5.2 μM in comparison with the EVs-MDA 1 μg/mL control. The percentage of clearance in the apical side encompasses the recovery in the basolateral side, for both EVs-MDA 1 μg/mL and EVs-MDA 1 μg/mL + vCPP2319 5.2 μM, suggesting that the translocation of the BBB by EVs-MDA alone or in combination with vCPP2319 occurs without retention in BBB cells. Interestingly, a different behavior was observed when analyzing the vCPP2319 translocation of the BBB (λ647/666). While vCPP2319 5.2 μM control showed a much lower percentage of recovery in the basolateral side (below 20 %), when combined with EVs-MDA 1 μg/mL, the percentage of recovery was significantly higher and very similar to that obtained for EVs-MDA 1 μg/mL + vCPP2319 5.2 μM or EVs-MDA 1 μg/mL at λ492/517. Importantly, these results demonstrate the ability of EVs-MDA to carry vCPP2319 across an *in vitro* monoculture BBB model. Moreover, since the percentage of vCPP2319 in the apical side is very similar for EVs-MDA 1 μg/mL + vCPP2319 5.2 μM and the peptide alone, the difference in the basolateral side translates into a significantly different percentage of retention in cells, which is much higher for the peptide control. This suggests that intracellular retention of vCPP2319 is the major cause for its inability to successfully translocate the BBB model. Overall, these results are striking as they unravel the ability of EVs-MDA to deliver vCPP2319 beyond an *in vitro* monoculture BBB model, which supports the use of these natural nano-sized vesicles as drug carriers capable of translocating the BBB.

It is worth stressing that the BBB model integrity was evaluated after the translocation assay using tetramethylrhodamine isothiocyanate-4 kDa dextran (RD4) (Fig. 5 – D). The results revealed no significant impact on the BBB model integrity after treatment with EVs-MDA 1 μg/mL combined with vCPP2319 5.2 μM or respective components. Ethylene glycol tetraacetic acid (EGTA) was used as a negative control for BBB integrity. Therefore, we may exclude the paracellular route for BBB translocation of EVs-MDA alone or combined with vCPP2319. This is deemed important because evidence points do EVs being able to compromise tight junctions, hence leading to a more permeable BBB in some cases [22,88–90].

4. Conclusion

In this work, we successfully isolated EVs from human breast cells. Upon characterization of the obtained samples using TEM and flow cytometry, we confirmed the presence of heterogenous populations of EVs with favorable characteristics to constitute a DDS, both in terms of size and specific molecular markers, such as CD63 – an exosomal marker - and CD105 – associated to the metastization process and recently referred to as a potential biomarker for MBC [47,49,50,61–64]. Aiming for the loading of EVs-MDA with vCPP2319, the interaction between both was studied and a strong interaction was detected. vCPP2319 strongly interacts with EVs-MDA resulting in abrupt response signals in SPR sensorgrams and significant alterations in the zeta potential values of the EVs in the presence of the peptide. Additionally, by applying a dissociation model to the dissociation phase response data in the SPR sensorgrams, we could estimate the fraction of the peptide that is retained at the surface of EVs-MDA, which is approximately 60 %. This evidence supports the use of EVs-MDA in combination with vCPP2319 as a potential DDS for MBC treatment. Nevertheless, further pharmacokinetics studies must be conducted in order to characterize the stability of this potential DDS in physiological conditions, since EVs modifications with small molecules may change their properties [91].

The combination of EVs-MDA with vCPP2319 did not impact the peptide's cytotoxicity nor selectivity. Importantly, translocation assays using an *in vitro* monoculture BBB model revealed that, at variance with the peptide alone, it translocated when previously incubated with EVs-MDA. Therefore, and since there was no significant impact in the BBB model integrity upon EVs-MDA + vCPP2319 translocation, EVs-MDA have the potential to safely carry the ACP vCPP2319 across the BBB. In conclusion, in a broader sense, the use of EVs obtained from TNBC cells cultures are promising carriers of anticancer drugs, with the potential to translocate the BBB and reach the brain parenchyma.

CRediT authorship contribution statement

Filipa D. Oliveira: Writing – original draft, Project administration, Methodology, Investigation, Formal analysis, Data curation, Conceptualization. **Marco Cavaco:** Writing – review & editing, Investigation, Formal analysis, Conceptualization, Writing – review & editing, Supervision, Project administration, Methodology, Funding acquisition, Formal analysis, Conceptualization. **Tiago N. Figueira:** Writing – review & editing, Methodology, Conceptualization. **Patrícia Napoleão:** Writing – review & editing, Resources, Methodology. **Javier Valle:** Writing – review & editing, Investigation. **Vera Neves:** Writing – review & editing, Methodology, Conceptualization. **David Andreu:** Writing – review & editing, Resources, Project administration, Funding acquisition.

Data availability statement

Data will be made available on request.

Declaration of competing interest

The authors declare that they have no known competing financial interests or personal relationships that could have appeared to influence the work reported in this paper.

Acknowledgements

Appendix A. Supplementary data

Supplementary data to this article can be found online at https://doi.org/10.1016/j.heliyon.2024.e40907.

References

[1] A. Steindl, A.S. Berghoff, Brain metastases in metastatic cancer: a review of recent advances in systemic therapies, Expert Rev. Anticancer Ther. 21 (2021) 325–339, https://doi.org/10.1080/14737140.2021.1851200.
[2] M.A. Proescholdt, P. Schödel, C. Doenitz, T. Pukrop, J. Höhne, N.O. Schmidt, K.-M. Schebesch, The management of brain metastases—systematic review of neurosurgical aspects, Cancers 13 (2021) 1616, https://doi.org/10.3390/cancers13071616.
[3] C. Nolan, L.M. Deangelis, Overview of metastatic disease of the central nervous system, Handb. Clin. Neurol. 149 (2018) 3–23, https://doi.org/10.1016/B978-0-12-811161-1.00001-3.
[4] A.S. Achrol, R.C. Rennert, C. Anders, R. Soffietti, M.S. Ahluwalia, L. Nayak, S. Peters, N.D. Arvold, G.R. Harsh, P.S. Steeg, S.D. Chang, Brain metastases, Nat. Rev. Dis. Prim. 5 (2019) 5, https://doi.org/10.1038/s41572-018-0055-y.
[5] J.H. Suh, R. Kotecha, S.T. Chao, M.S. Ahluwalia, A. Sahgal, E.L. Chang, Current approaches to the management of brain metastases, Nat. Rev. Clin. Oncol. 17 (2020) 279–299, https://doi.org/10.1038/s41571-019-0320-3.
[6] I. Witzel, L. Oliveira-Ferrer, K. Pantel, V. Müller, H. Wikman, Breast cancer brain metastases: biology and new clinical perspectives, Breast Cancer Res. 18 (2016) 8, https://doi.org/10.1186/s13058-015-0665-1.
[7] N. Niikura, N. Hayashi, N. Masuda, S. Takashima, R. Nakamura, K.I. Watanabe, C. Kanbayashi, M. Ishida, Y. Hozumi, M. Tsuneizumi, N. Kondo, Y. Naito, Y. Honda, A. Matsui, T. Fujisawa, R. Oshitanai, H. Yasojima, Y. Tokuda, S. Saji, H. Iwata, Treatment outcomes and prognostic factors for patients with brain metastases from breast cancer of each subtype: a multicenter retrospective analysis, Breast Cancer Res. Treat. 147 (2014) 103–112, https://doi.org/10.1007/s10549-014-3090-8.
[8] D. Wang, C. Wang, L. Wang, Y. Chen, A comprehensive review in improving delivery of small-molecule chemotherapeutic agents overcoming the blood-brain/brain tumor barriers for glioblastoma treatment, Drug Deliv. 26 (2019) 551–565, https://doi.org/10.1080/10717544.2019.1616235.
[9] R. Pandit, L. Chen, J. Götz, The blood-brain barrier: physiology and strategies for drug delivery, Adv. Drug Deliv. Rev. 165–166 (2020) 1–14, https://doi.org/10.1016/j.addr.2019.11.009.
[10] S. Milewska, K. Niemirowicz-Laskowska, G. Siemiaszko, P. Nowicki, A.Z. Wilczewska, H. Car, Current trends and challenges in pharmacoeconomic aspects of nanocarriers as drug delivery systems for cancer treatment, Int. J. Nanomed. 16 (2021) 6593–6644, https://doi.org/10.2147/IJN.S323831.
[11] C. Gutierrez-Millan, C. Calvo Díaz, J.M. Lanao, C.I. Colino, Advances in exosomes-based drug delivery systems, Macromol. Biosci. 21 (2021) 1–19, https://doi.org/10.1002/mabi.202000269.
[12] M.E.R. O'Brien, N. Wigler, M. Inbar, R. Rosso, E. Grischke, A. Santoro, R. Catane, D.G. Kieback, P. Tomczak, S.P. Ackland, F. Orlandi, L. Mellars, L. Alland, C. Tendler, Reduced cardiotoxicity and comparable efficacy in a phase III trial of pegylated liposomal doxorubicin HCl (CAELYX^{TM}/Doxil®) versus conventional doxorubicin for first-line treatment of metastatic breast cancer, Ann. Oncol. 15 (2004) 440–449, https://doi.org/10.1093/annonc/mdh097.
[13] N. Tominaga, Y. Yoshioka, T. Ochiya, A novel platform for cancer therapy using extracellular vesicles, Adv. Drug Deliv. Rev. 95 (2015) 50–55, https://doi.org/10.1016/j.addr.2015.10.002.
[14] M. Hadla, S. Palazzolo, G. Corona, I. Caligiuri, V. Canzonieri, G. Toffoli, F. Rizzolio, Exosomes increase the therapeutic index of doxorubicin in breast and ovarian cancer mouse models, Nanomedicine 11 (2016) 2431–2441, https://doi.org/10.2217/nnm-2016-0154.
[15] X. Luan, K. Sansanaphongpricha, I. Myers, H. Chen, H. Yuan, D. Sun, Engineering exosomes as refined biological nanoplatforms for drug delivery, Acta Pharmacol. Sin. 38 (2017) 754–763, https://doi.org/10.1038/aps.2017.12.
[16] E. Cocucci, J. Meldolesi, Ectosomes and exosomes: shedding the confusion between extracellular vesicles, Trends Cell Biol. 25 (2015) 364–372, https://doi.org/10.1016/j.tcb.2015.01.004.
[17] M. Zheng, M. Huang, X. Ma, H. Chen, X. Gao, Harnessing exosomes for the development of brain drug delivery systems, Bioconjugate Chem. 30 (2019) 994–1005, https://doi.org/10.1021/acs.bioconjchem.9b00085.
[18] I. Wortzel, S. Dror, C.M. Kenific, D. Lyden, Exosome-Mediated metastasis: communication from a distance, Dev. Cell 49 (2019) 347–360, https://doi.org/10.1016/j.devcel.2019.04.011.
[19] G. Van Niel, G. D'Angelo, G. Raposo, Shedding light on the cell biology of extracellular vesicles, Nat. Rev. Mol. Cell Biol. 19 (2018) 213–228, https://doi.org/10.1038/nrm.2017.125.
[20] D. dan Yu, Y. Wu, H. yu Shen, M. meng Lv, W. xian Chen, X. hui Zhang, S. liang Zhong, J. hai Tang, J. hua Zhao, Exosomes in development, metastasis and drug resistance of breast cancer, Cancer Sci. 106 (2015) 959–964, https://doi.org/10.1111/cas.12715.
[21] M. Zheng, M. Huang, H. Chen, X. Gao, Harnessing exosomes for the development of brain drug delivery systems. https://doi.org/10.1021/acs.bioconjchem.9b00085, 2019.
[22] F.D. Oliveira, M.A.R.B. Castanho, V. Neves, Exosomes and brain metastases: a review on their role and potential applications, Int. J. Mol. Sci. 22 (2021) 10899, https://doi.org/10.3390/ijms221910899.
[23] D. Ha, N. Yang, V. Nadithe, A.B. Pharmaceutica, Sinica, Exosomes as therapeutic drug carriers and delivery vehicles across biological membranes: current perspectives and future challenges, Acta Pharm. Sin. B 6 (2016) 287–296, https://doi.org/10.1016/j.apsb.2016.02.001.

[24] L. Qiao, S. Hu, K. Huang, T. Su, Z. Li, A. Vandergriff, J. Cores, P.U. Dinh, T. Allen, D. Shen, H. Liang, Y. Li, K. Cheng, Tumor cell-derived exosomes home to their cells of origin and can be used as Trojan horses to deliver cancer drugs, Theranostics 10 (2020) 3474–3487, https://doi.org/10.7150/thno.39434.

[25] C. Gutierrez-Millan, C. Calvo Díaz, J.M. Lanao, C.I. Colino, Advances in exosomes-based drug delivery systems, Macromol. Biosci. 21 (2021) 2000269, https://doi.org/10.1002/mabi.202000269.

[26] H. Saari, E. Lázaro-Ibáñez, T. Viitala, E. Vuorimaa-Laukkanen, P. Siljander, M. Yliperttula, Microvesicle- and exosome-mediated drug delivery enhances the cytotoxicity of Paclitaxel in autologous prostate cancer cells, J. Contr. Release 220 (2015) 727–737, https://doi.org/10.1016/j.jconrel.2015.09.031.

[27] H. Liu, M. Shen, D. Zhao, D. Ru, Y. Duan, C. Ding, H. Li, The effect of triptolide-loaded exosomes on the proliferation and apoptosis of human ovarian cancer SKOV3 cells, BioMed Res. Int. 2019 (2019), https://doi.org/10.1155/2019/2595801.

[28] Y. Ma, Z. Yang, K. Huntoon, W. Jiang, B.Y.S. Kim, Advanced immunotherapy approaches for glioblastoma, Adv. Ther. 4 (2021), https://doi.org/10.1002/adtp.202100046.

[29] M. Zhang, S. Hu, L. Liu, P. Dang, Y. Liu, Z. Sun, B. Qiao, C. Wang, Engineered exosomes from different sources for cancer-targeted therapy, Signal Transduct. Targeted Ther. 8 (2023) 124, https://doi.org/10.1038/s41392-023-01382-y.

[30] F.D. Oliveira, M. Cavaco, T.N. Figueira, J. Valle, V. Neves, D. Andreu, D. Gaspar, M.A.R.B. Castanho, The antimetastatic breast cancer activity of the viral protein-derived peptide vCPP2319 as revealed by cellular biomechanics, FEBS J. 289 (2022) 1603–1624, https://doi.org/10.1111/febs.16247.

[31] J.M. Freire, S. Almeida Dias, L. Flores, A.S. Veiga, M.A.R.B. Castanho, Mining viral proteins for antimicrobial and cell-penetrating drug delivery peptides, Bioinformatics 31 (2015) 2252–2256, https://doi.org/10.1093/bioinformatics/btv131.

[32] Ü. Langel, Therapeutic potential of CPPs, in: CPP, Cell-Penetrating Pept, Springer Singapore, Singapore, 2019, pp. 409–461, https://doi.org/10.1007/978-981-13-8747-0_12.

[33] D.W. Hoskin, A. Ramamoorthy, Studies on anticancer activities of antimicrobial peptides, Biochim. Biophys. Acta Biomembr. 1778 (2008) 357–375, https://doi.org/10.1016/j.bbamem.2007.11.008.

[34] T.N. Figueira, F.D. Oliveira, I. Almeida, É.O. Mello, V.M. Gomes, M.A.R.B. Castanho, D. Gaspar, Challenging metastatic breast cancer with the natural defensin PvD 1, Nanoscale 9 (2017) 16887–16899, https://doi.org/10.1039/C7NR05872A.

[35] M. Cavaco, C. Pérez-peinado, J. Valle, R.D.M. Silva, To What Extent Do Fluorophores Bias the Biological Activity of Peptides ? A Practical Approach Using Membrane-Active Peptides as Models 8 (2020), https://doi.org/10.3389/fbioe.2020.552035.

[36] S.G. Antimisiaris, S. Mourtas, A. Marazioti, Exosomes and exosome-inspired vesicles for targeted drug delivery, Pharmaceutics 10 (2018), https://doi.org/10.3390/pharmaceutics10040218.

[37] C. Théry, K.W. Witwer, E. Aikawa, M.J. Alcaraz, J.D. Anderson, R. Andriantsitohaina, A. Antoniou, T. Arab, F. Archer, G.K. Atkin-Smith, D.C. Ayre, J.-M. Bach, D. Bachurski, H. Baharvand, L. Balaj, S. Baldacchino, N.N. Bauer, A.A. Baxter, M. Bebawy, C. Beckham, A. Bedina Zavec, A. Benmoussa, A.C. Berardi, P. Bergese, E. Bielska, C. Blenkiron, S. Bobis-Wozowicz, E. Boilard, W. Boireau, A. Bongiovanni, F.E. Borràs, S. Bosch, C.M. Boulanger, X. Breakefield, A.M. Breglio, M.Á. Brennan, D.R. Brigstock, A. Brisson, M.L.D. Broekman, J.F. Bromberg, P. Bryl-Górecka, S. Buch, A.H. Buck, D. Burger, S. Busatto, D. Buschmann, B. Bussolati, E.I. Buzás, J.B. Byrd, G. Camussi, D.R.F. Carter, S. Caruso, L.W. Chamley, Y.-T. Chang, C. Chen, S. Chen, L. Cheng, A.R. Chin, A. Clayton, S. P. Clerici, A. Cocks, E. Cocucci, R.J. Coffey, A. Cordeiro-da-Silva, Y. Couch, F.A.W. Coumans, B. Coyle, R. Crescitelli, M.F. Criado, C. D'Souza-Schorey, S. Das, A. Datta Chaudhuri, P. de Candia, E.F. De Santana, O. De Wever, H.A. del Portillo, T. Demaret, S. Deville, A. Devitt, B. Dhondt, D. Di Vizio, L.C. Dieterich, V. Dolo, A.P. Dominguez Rubio, M. Dominici, M.R. Dourado, T.A.P. Driedonks, F.V. Duarte, H.M. Duncan, R.M. Eichenberger, K. Ekström, S. El Andaloussi, C. Elie-Caille, U. Erdbrügger, J.M. Falcón-Pérez, F. Fatima, J.E. Fish, M. Flores-Bellver, A. Försönits, A. Frelet-Barrand, F. Fricke, G. Fuhrmann, S. Gabrielsson, A. Gámez-Valero, C. Gardiner, K. Gärtner, R. Gaudin, Y.S. Gho, B. Giebel, C. Gilbert, M. Gimona, I. Giusti, D.C.I. Goberdhan, A. Görgens, S.M. Gorski, D. W. Greening, J.C. Gross, A. Gualerzi, G.N. Gupta, D. Gustafson, A. Handberg, R.A. Haraszti, P. Harrison, H. Hegyesi, A. Hendrix, A.F. Hill, F.H. Hochberg, K. F. Hoffmann, B. Holder, H. Holthofer, B. Hosseinkhani, G. Hu, Y. Huang, V. Huber, S. Hunt, A.G.-E. Ibrahim, T. Ikezu, J.M. Inal, M. Isin, A. Ivanova, H. K. Jackson, S. Jacobsen, S.M. Jay, M. Jayachandran, G. Jenster, L. Jiang, S.M. Johnson, J.C. Jones, A. Jong, T. Jovanovic-Talisman, S. Jung, R. Kalluri, S. Kano, S. Kaur, Y. Kawamura, E.T. Keller, D. Khamari, E. Khomyakova, A. Khvorova, P. Kierulf, K.P. Kim, T. Kislinger, M. Klingeborn, D.J. Klinke, M. Kornek, M. M. Kosanović, Á.F. Kovács, E.-M. Krämer-Albers, S. Krasemann, M. Krause, I.V. Kurochkin, G.D. Kusuma, S. Kuypers, S. Laitinen, S.M. Langevin, L.R. Languino, J. Lannigan, C. Lässer, L.C. Laurent, G. Lavieu, E. Lázaro-Ibáñez, S. Le Lay, M.-S. Lee, Y.X.F. Lee, D.S. Lemos, M. Lenassi, A. Leszczynska, I.T.S. Li, K. Liao, S. F. Libregts, E. Ligeti, R. Lim, S.K. Lim, A. Linē, K. Linnemannstöns, A. Llorente, C.A. Lombard, M.J. Lorenowicz, Á.M. Lörincz, J. Lötvall, J. Lovett, M.C. Lowry, X. Loyer, Q. Lu, B. Lukomska, T.R. Lunavat, S.L.N. Maas, H. Malhi, A. Marcilla, J. Mariani, J. Mariscal, E.S. Martens-Uzunova, L. Martin-Jaular, M.C. Martinez, V.R. Martins, S. Mathivanan, M. Mathieu, S. Mathivanan, M. Maugeri, L.K. McGinnis, M.J. McVey, D.G. Meckes, K.L. Meehan, I. Mertens, V.R. Minciacchi, A. Möller, M. Møller Jørgensen, A. Morales-Kastresana, J. Morhayim, F. Mullier, M. Muraca, L. Musante, V. Mussack, D.C. Muth, K.H. Myburgh, T. Najrana, M. Nawaz, I. Nazarenko, P. Nejsum, C. Neri, T. Neri, R. Nieuwland, L. Nimrichter, J.P. Nolan, E.N. Nolte-'t Hoen, N. Noren Hooten, L. O'Driscoll, T. O'Grady, A. O'Loghlen, T. Ochiya, M. Olivier, A. Ortiz, L.A. Ortiz, X. Osteikoetxea, O. Østergaard, M. Ostrowski, J. Park, D.M. Pegtel, H. Peinado, F. Perut, M.W. Pfaffl, D.G. Phinney, D. H. Pieters, R.C. Pink, D.S. Pisetsky, E. Pogge von Strandmann, I. Polakovicova, I.K.H. Poon, B.H. Powell, I. Prada, L. Pulliam, P. Quesenberry, A. Radeghieri, R. L. Raffai, S. Raimondo, J. Rak, M.I. Ramirez, G. Raposo, M.S. Rayyan, N. Regev-Rudzki, F.L. Ricklefs, P.D. Robbins, D.D. Roberts, S.C. Rodrigues, E. Rohde, S. Rome, K.M.A. Rouschop, A. Rughetti, A.E. Russell, P. Saá, S. Sahoo, E. Salas-Huenuleo, C. Sánchez, J.A. Saugstad, M.J. Saul, R.M. Schiffelers, R. Schneider, T. H. Schøyen, A. Scott, E. Shahaj, S. Sharma, O. Shatnyeva, F. Shekari, G.V. Shelke, A.K. Shetty, K. Shiba, P.R.M. Siljander, A.M. Silva, A. Skowronek, O.L. Snyder, R.P. Soares, B.W. Sódar, C. Soekmadji, J. Sotillo, P.D. Stahl, W. Stoorvogel, S.L. Stott, E.F. Strasser, S. Swift, H. Tahara, M. Tewari, K. Timms, S. Tiwari, R. Tixeira, M. Tkach, W.S. Toh, R. Tomasini, A.C. Torrecilhas, J.P. Tosar, V. Toxavidis, L. Urbanelli, P. Vader, B.W.M. van Balkom, S.G. van der Grein, J. Van Deun, M.J.C. van Herwijnen, K. Van Keuren-Jensen, G. van Niel, M.E. van Royen, A.J. van Wijnen, M.H. Vasconcelos, I.J. Vechetti, T.D. Veit, L.J. Vella, É. Velot, F.J. Verweij, B. Vestad, J.L. Viñas, T. Visnovitz, K.V. Vukman, J. Wahlgren, D.C. Watson, M.H.M. Wauben, A. Weaver, J.P. Webber, V. Weber, A.M. Wehman, D. J. Weiss, J.A. Welsh, S. Wendt, A.M. Wheelock, Z. Wiener, L. Witte, J. Wolfram, A. Xagorari, P. Xander, J. Xu, X. Yan, M. Yáñez-Mó, H. Yin, Y. Yuana, V. Zappulli, J. Zarubova, V. Žékas, J. Zhang, Z. Zhao, L. Zheng, A.R. Zheutlin, A.M. Zickler, P. Zimmermann, A.M. Zivkovic, D. Zocco, E.K. Zuba-Surma, Minimal information for studies of extracellular vesicles 2018 (MISEV2018): a position statement of the International Society for Extracellular Vesicles and update of the MISEV2014 guidelines, J. Extracell. Vesicles 7 (2018) 1535750, https://doi.org/10.1080/20013078.2018.1535750.

[38] E. Beit-yannai, S. Tabak, W.D. Stamer, Physical exosome : exosome interactions Introduction / Background 22 (2018) 2001–2006, https://doi.org/10.1111/jcmm.13479.

[39] T. Yamashita, Y. Takahashi, M. Nishikawa, Y. Takakura, Effect of exosome isolation methods on physicochemical properties of exosomes and clearance of exosomes from the blood circulation, Eur. J. Pharm. Biopharm. 98 (2016) 1–8, https://doi.org/10.1016/j.ejpb.2015.10.017.

[40] C. Gardiner, M. Shaw, P. Hole, J. Smith, C.W. Redman, I.L. Sargent, C. Gardiner, M. Shaw, P. Hole, J. Smith, D. Tannetta, C.W. Redman, I.L. Sargent, C. Gardiner, M. Shaw, P. Hole, J. Smith, D. Tannetta, C.W. Redman, I.L. Sargent, Measurement of refractive index by nanoparticle tracking analysis reveals heterogeneity in extracellular vesicles (2014) 3078, https://doi.org/10.3402/jev.v3.25361.

[41] H. Zhang, D. Freitas, H.S. Kim, K. Fabijanic, Z. Li, H. Chen, M.T. Mark, H. Molina, A.B. Martin, L. Bojmar, J. Fang, S. Rampersaud, A. Hoshino, I. Matei, C. M. Kenific, M. Nakajima, A.P. Mutvei, P. Sansone, W. Buehring, H. Wang, J.P. Jimenez, L. Cohen-Gould, N. Paknejad, M. Brendel, K. Manova-Todorova, A. Magalhães, J.A. Ferreira, H. Osório, A.M. Silva, A. Massey, J.R. Cubillos-Ruiz, G. Galletti, P. Giannakakou, A.M. Cuervo, J. Blenis, R. Schwartz, M.S. Brady, H. Peinado, J. Bromberg, H. Matsui, C.A. Reis, D. Lyden, Identification of distinct nanoparticles and subsets of extracellular vesicles by asymmetric flow field-flow fractionation, Nat. Cell Biol. 20 (2018) 332–343, https://doi.org/10.1038/s41556-018-0040-4.

[42] M.Y. Fong, W. Zhou, L. Liu, A.Y. Alontaga, M. Chandra, J. Ashby, A. Chow, S.T.F. O'Connor, S. Li, A.R. Chin, G. Somlo, M. Palomares, Z. Li, J.R. Tremblay, A. Tsuyada, G. Sun, M.A. Reid, X. Wu, P. Swiderski, X. Ren, Y. Shi, M. Kong, W. Zhong, Y. Chen, S.E. Wang, Breast-cancer-secreted miR-122 reprograms glucose metabolism in premetastatic niche to promote metastasis, Nat. Cell Biol. 17 (2015) 183–194, https://doi.org/10.1038/ncb3094.

[43] Z. Rafighdoust, J. Baharara, M.M. Forghanifard, M.A. Kerachian, Isolation and characterization of exosomes derived from breast cancer MDA-MB-231 cell line, Gene, Cell Tissue 8 (2021) 6–11, https://doi.org/10.5812/gct.110505.

[44] S. Keller, J. Ridinger, A.-K. Rupp, J.W.G. Janssen, P. Altevogt, Body fluid derived exosomes as a novel template for clinical diagnostics, J. Transl. Med. 9 (2011) 86, https://doi.org/10.1186/1479-5876-9-86.

[45] F. Ender, P. Zamzow, N. von Bubnoff, F. Gieseler, Detection and quantification of extracellular vesicles via FACS: membrane labeling matters, Int. J. Mol. Sci. 21 (2020), https://doi.org/10.3390/ijms21010291.

[46] V. Pospichalova, J. Svoboda, Z. Dave, A. Kotrbova, K. Kaiser, D. Klemova, L. Ilkovics, A. Hampl, I. Crha, E. Jandakova, L. Minar, V. Weinberger, V. Bryja, Simplified protocol for flow cytometry analysis of fluorescently labeled exosomes and microvesicles using dedicated flow cytometer, J. Extracell. Vesicles 4 (2015) 1–15, https://doi.org/10.3402/jev.v4.25530.

[47] G. Kibria, E.K. Ramos, Y. Wan, D.R. Gius, H. Liu, Exosomes as a drug delivery system in cancer therapy: potential and challenges, Mol. Pharm. 15 (2018) 3625–3633, https://doi.org/10.1021/acs.molpharmaceut.8b00277.

[48] S. El Andaloussi, I. Mäger, X.O. Breakefield, M.J.A. Wood, Extracellular vesicles: biology and emerging therapeutic opportunities, Nat. Rev. Drug Discov. 12 (2013) 347–357, https://doi.org/10.1038/nrd3978.

[49] A. Bobrie, C. Thery, Exosomes and communication between tumours and the immune system: are all exosomes equal? Biochem. Soc. Trans. 41 (2013) 263–267, https://doi.org/10.1042/BST20120245.

[50] S.R. Douglas, K.T. Yeung, J. Yang, S.L. Blair, O. Cohen, B.P. Eliceiri, Identification of CD105+ extracellular vesicles as a candidate biomarker for metastatic breast cancer, J. Surg. Res. 268 (2021) 168–173, https://doi.org/10.1016/j.jss.2021.06.050.

[51] C. Li, B. Guo, P.B. Wilson, A. Stewart, G. Byrne, N. Bundred, S. Kumar, Plasma levels of soluble CD105 correlate with metastasis in patients with breast cancer, Int. J. Cancer 86 (2000) 122–126, https://doi.org/10.1002/(sici)1097-0215(20000320)89:2<122::aid-ijc4>3.0.co;2-m.

[52] S.E. Duff, C. Li, J.M. Garland, S. Kumar, CD105 is important for angiogenesis: evidence and potential applications, Faseb. J. 17 (2003) 984–992, https://doi.org/10.1096/fj.02-0634rev.

[53] A.B. Lyons, Analysing cell division in vivo and in vitro using flow cytometric measurement of CFSE dye dilution, J. Immunol. Methods 243 (2000) 147–154, https://doi.org/10.1016/S0022-1759(00)00231-3.

[54] F. Ma, H. Li, H. Wang, X. Shi, Y. Fan, X. Ding, C. Lin, Q. Zhan, H. Qian, B. Xu, Enriched CD44+/CD24- population drives the aggressive phenotypes presented in triple-negative breast cancer (TNBC), Cancer Lett. 353 (2014) 153–159, https://doi.org/10.1016/j.canlet.2014.06.022.

[55] K.J. Chavez, S.V. Garimella, S. Lipkowitz, Triple negative breast cancer cell lines: one tool in the search for better treatment of triple negative breast cancer, Breast Dis. 32 (2011) 35–48, https://doi.org/10.3233/BD-2010-0307.

[56] D.-H. Bach, J.-Y. Hong, H.J. Park, S.K. Lee, The role of exosomes and miRNAs in drug-resistance of cancer cells, Int. J. Cancer (2017) 1–11, https://doi.org/10.1002/ijc.30669, 00.

[57] D.D. Taylor, C. Gercel-Taylor, MicroRNA signatures of tumor-derived exosomes as diagnostic biomarkers of ovarian cancer, Gynecol. Oncol. 110 (2008) 13–21, https://doi.org/10.1016/j.ygyno.2008.04.033.

[58] P. Kharaziha, S. Ceder, Q. Li, T. Panaretakis, Tumor cell-derived exosomes: a message in a bottle, Biochim. Biophys. Acta Rev. Canc 1826 (2012) 103–111, https://doi.org/10.1016/j.bbcan.2012.03.006.

[59] A.-K. Rupp, C. Rupp, S. Keller, J.C. Brase, R. Ehehalt, M. Fogel, G. Moldenhauer, F. Marmé, H. Sültmann, P. Altevogt, Loss of EpCAM expression in breast cancer derived serum exosomes: role of proteolytic cleavage, Gynecol. Oncol. 122 (2011) 437–446, https://doi.org/10.1016/j.ygyno.2011.04.035.

[60] S. Kruger, Z.Y. Abd Elmageed, D.H. Hawke, P.M. Wörner, D.A. Jansen, A.B. Abdel-Mageed, E.U. Alt, R. Izadpanah, Molecular characterization of exosome-like vesicles from breast cancer cells, BMC Cancer 14 (2014) 44, https://doi.org/10.1186/1471-2407-14-44.

[61] S. El Andaloussi, S. Lakhal, I. Mäger, M.J.A. Wood, Exosomes for targeted siRNA delivery across biological barriers, Adv. Drug Deliv. Rev. 65 (2013) 391–397, https://doi.org/10.1016/j.addr.2012.08.008.

[62] J. Skalska, F.D. Oliveira, T.N. Figueira, É.O. Mello, V.M. Gomes, G. McNaughton-Smith, M.A.R.B. Castanho, D. Gaspar, Plant defensin Pv D 1 modulates the membrane composition of breast tumour-derived exosomes, Nanoscale 11 (2019) 23366–23381, https://doi.org/10.1039/C9NR07843F.

[63] M. de Almeida Fuzeta, N. Bernardes, F.D. Oliveira, A.C. Costa, A. Fernandes-Platzgummer, J.P. Farinha, C.A.V. Rodrigues, S. Jung, R.-J. Tseng, W. Milligan, B. Lee, M.A.R.B. Castanho, D. Gaspar, J.M.S. Cabral, C.L. da Silva, Scalable production of human mesenchymal stromal cell-derived extracellular vesicles under serum-/xeno-free conditions in a microcarrier-based bioreactor culture system, Front. Cell Dev. Biol. 8 (2020), https://doi.org/10.3389/fcell.2020.553444.

[64] C. Grange, M. Tapparo, F. Collino, L. Vitillo, C. Damasco, M.C. Deregibus, C. Tetta, B. Bussolati, G. Camussi, Microvesicles released from human renal cancer stem cells stimulate angiogenesis and formation of lung premetastatic niche, Cancer Res. 71 (2011) 5346–5356, https://doi.org/10.1158/0008-5472.CAN-11-0241.

[65] T.N. Figueira, J.M. Freire, C. Cunha-Santos, M. Heras, J. Gonçalves, A. Moscona, M. Porotto, A. Salomé Veiga, M.A.R.B. Castanho, Quantitative analysis of molecular partition towards lipid membranes using surface plasmon resonance, Sci. Rep. 7 (2017) 1–10, https://doi.org/10.1038/srep45647.

[66] D.J. Craik, S.T. Henriques, J.S. Mylne, C.K. Wang, Cyclotide isolation and characterization, Methods Enzymol. 516 (2012) 37–62, https://doi.org/10.1016/B978-0-12-394291-3.00024-1.

[67] V. Hodnik, G. Anderluh, Lipid-Protein Interactions, Humana Press, Totowa, NJ, 2013, https://doi.org/10.1007/978-1-62703-275-9.

[68] M. Beseničar, P. Maček, J.H. Lakey, G. Anderluh, Surface plasmon resonance in protein-membrane interactions, Chem. Phys. Lipids 141 (2006) 169–178, https://doi.org/10.1016/j.chemphyslip.2006.02.010.

[69] A. Thakur, G. Qiu, S.P. Ng, J. Guan, J. Yue, Y. Lee, C.M.L. Wu, Direct detection of two different tumor-derived extracellular vesicles by SAM-AuNIs LSPR biosensor, Biosens. Bioelectron. 94 (2017) 400–407, https://doi.org/10.1016/j.bios.2017.03.036.

[70] Z. Mao, J. Zhao, J. Chen, X. Hu, K. Koh, H. Chen, A simple and direct SPR platform combining three-in-one multifunctional peptides for ultra-sensitive detection of PD-L1 exosomes, Sensor. Actuator. B Chem. 346 (2021) 130496, https://doi.org/10.1016/j.snb.2021.130496.

[71] Y. Wang, Z. Mao, Q. Chen, K. Koh, X. Hu, H. Chen, Rapid and sensitive detection of PD-L1 exosomes using Cu-TCPP 2D MOF as a SPR sensitizer, Biosens. Bioelectron. 201 (2022) 113954, https://doi.org/10.1016/j.bios.2021.113954.

[72] A.A.I. Sina, R. Vaidyanathan, S. Dey, L.G. Carrascosa, M.J.A. Shiddiky, M. Trau, Real time and label free profiling of clinically relevant exosomes, Sci. Rep. 6 (2016) 1–9, https://doi.org/10.1038/srep30460.

[73] A.A.I. Sina, R. Vaidyanathan, A. Wuethrich, L.G. Carrascosa, M. Trau, Label-free detection of exosomes using a surface plasmon resonance biosensor, Anal. Bioanal. Chem. 411 (2019) 1311–1318, https://doi.org/10.1007/s00216-019-01608-5.

[74] Y. Sun, C. Huo, Z. Qiao, Z. Shang, A. Uzzaman, S. Liu, X. Jiang, L.Y. Fan, L. Ji, X. Guan, C.X. Cao, H. Xiao, Comparative proteomic analysis of exosomes and microvesicles in human saliva for lung cancer, J. Proteome Res. 17 (2018) 1101–1107, https://doi.org/10.1021/acs.jproteome.7b00770.

[75] T. Yang, P. Martin, B. Fogarty, A. Brown, K. Schurman, R. Phipps, V.P. Yin, P. Lockman, S. Bai, Exosome delivered anticancer drugs across the blood-brain barrier for brain cancer therapy in Danio rerio, Pharm. Res. (N. Y.) 32 (2015) 2003–2014, https://doi.org/10.1007/s11095-014-1593-y.

[76] D. Sun, X. Zhuang, X. Xiang, Y. Liu, S. Zhang, C. Liu, S. Barnes, W. Grizzle, D. Miller, H.-G. Zhang, A novel nanoparticle drug delivery system: the anti-inflammatory activity of curcumin is enhanced when encapsulated in exosomes, Mol. Ther. 18 (2010) 1606–1614, https://doi.org/10.1038/mt.2010.105.

[77] X. Zhuang, X. Xiang, W. Grizzle, D. Sun, S. Zhang, R.C. Axtell, S. Ju, J. Mu, L. Zhang, L. Steinman, D. Miller, H.G. Zhang, Treatment of brain inflammatory diseases by delivering exosome encapsulated anti-inflammatory drugs from the nasal region to the brain, Mol. Ther. 19 (2011) 1769–1779, https://doi.org/10.1038/mt.2011.164.

[78] G. Fuhrmann, A. Serio, M. Mazo, R. Nair, M.M. Stevens, Active loading into extracellular vesicles significantly improves the cellular uptake and photodynamic effect of porphyrins, J. Contr. Release 205 (2015) 35–44, https://doi.org/10.1016/j.jconrel.2014.11.029.

[79] M. Kesimer, R. Gupta, Physical characterization and profiling of airway epithelial derived exosomes using light scattering, Methods 87 (2015) 59–63, https://doi.org/10.1016/j.ymeth.2015.03.013.

[80] V. Sokolova, A.-K. Ludwig, S. Hornung, O. Rotan, P.A. Horn, M. Epple, B. Giebel, Characterisation of exosomes derived from human cells by nanoparticle tracking analysis and scanning electron microscopy, Colloids Surf. B Biointerfaces 87 (2011) 146–150, https://doi.org/10.1016/j.colsurfb.2011.05.013.

[81] D. Rupert, V. Claudio, C. Lässer, M. Bally, Methods for the physical characterization and quantification of extracellular vesicles in biological samples, Biochim. Biophys. Acta Gen. Subj. (2016), https://doi.org/10.1016/j.bbagen.2016.07.028.

[82] T. Akagi, K. Kato, N. Hanamura, M. Kobayashi, T. Ichiki, Evaluation of desialylation effect on zeta potential of extracellular vesicles secreted from human prostate cancer cells by on-chip microcapillary electrophoresis, Jpn. J. Appl. Phys. 53 (2014), https://doi.org/10.7567/JJAP.53.06JL01.

[83] J.L. Hood, M.J. Scott, S.A. Wickline, Maximizing exosome colloidal stability following electroporation, Anal. Biochem. 448 (2014) 41–49, https://doi.org/10.1016/j.ab.2013.12.001.

[84] K. Kato, M. Kobayashi, N. Hanamura, T. Akagi, N. Kosaka, T. Ochiya, T. Ichiki, Electrokinetic evaluation of individual exosomes by on-chip microcapillary electrophoresis with laser dark-field microscopy, Jpn. J. Appl. Phys. 52 (2013), https://doi.org/10.7567/JJAP.52.06GK10.

[85] R.O. Elliott, M. He, Unlocking the power of exosomes for crossing biological barriers in drug delivery, Pharmaceutics 13 (2021) 1–20, https://doi.org/10.3390/pharmaceutics13010122.

[86] W.M. Pardridge, The blood-brain barrier and neurotherapeutics, NeuroRx 2 (2005) 1–2, https://doi.org/10.1602/neurorx.2.1.1.

[87] L. Alvarez-Erviti, Y. Seow, H. Yin, C. Betts, S. Lakhal, M.J.A. Wood, Delivery of siRNA to the mouse brain by systemic injection of targeted exosomes, Nat. Biotechnol. 29 (2011) 341–345, https://doi.org/10.1038/nbt.1807.

[88] N. Tominaga, N. Kosaka, M. Ono, T. Katsuda, Y. Yoshioka, K. Tamura, J. Lötvall, H. Nakagama, T. Ochiya, Brain metastatic cancer cells release microRNA-181c-containing extracellular vesicles capable of destructing blood-brain barrier, Nat. Commun. 6 (2015), https://doi.org/10.1038/ncomms7716.

[89] Y. Lu, L. Chen, L. Li, Y. Cao, Exosomes derived from brain metastatic breast cancer cells destroy the blood-brain barrier by carrying lncRNA GS1-600g8.5, BioMed Res. Int. 2020 (2020), https://doi.org/10.1155/2020/7461727.

[90] W. Zhou, M.Y. Fong, Y. Min, G. Somlo, L. Liu, M.R. Palomares, Y. Yu, A. Chow, S.T.F. O'Connor, A.R. Chin, Y. Yen, Y. Wang, E.G. Marcusson, P. Chu, J. Wu, X. Wu, A.X. Li, Z. Li, H. Gao, X. Ren, M.P. Boldin, P.C. Lin, S.E. Wang, Cancer-Secreted miR-105 destroys vascular endothelial barriers to promote metastasis, Cancer Cell 25 (2014) 501–515, https://doi.org/10.1016/j.ccr.2014.03.007.

[91] M. Heidarzadeh, A. Zarebkohan, R. Rahbarghazi, E. Sokullu, Protein corona and exosomes: new challenges and prospects, Cell Commun. Signal. 21 (2023) 64, https://doi.org/10.1186/s12964-023-01089-1.